JOURNAL OF GEOPHYSICAL RESEARCH, VOL. 114, B12405, doi:10.1029/2008JB006194, 2009

Constrained potential field modeling of the crustal architecture of the Musgrave Province in central Australia: Evidence for lithospheric strengthening due to crust-mantle boundary uplift

Alan R. A. Aitken,[1] Peter G. Betts,[1] Roberto F. Weinberg,[1] and Daniel Gray[2]

Received 5 November 2008; revised 11 June 2009; accepted 19 August 2009; published 23 December 2009.

[1] We image the crustal architecture of the Musgrave Province with petrophysically constrained forward models of new potential field data. These models image divergent shallow-dipping crustal scale thrusts that, at depth, link with an axial zone defined by steeper, lithospheric scale transpressional shear zones. They also show that to permit a near-surface density distribution that is consistent with petrophysical and geological observations, approximately 15–20 km of crust-mantle boundary uplift is necessary beneath the axial zone. The long-term preservation of this crust-mantle boundary offset implies a change from relatively weak lithosphere to relatively strong lithosphere during the intraplate Petermann Orogeny. To explain this, we propose a model in which uplift of the axial zone of the orogen leads to local lithospheric strengthening as a result of the uplift of mantle rocks into the lower crust, coupled with long-term lithospheric cooling due to the erosion of a radioactive upper crust. Brace-Goetze lithospheric strength models suggest that these processes may have increased the integrated strength of the lithosphere by a factor of 1.4–2.8. Because of this strengthening, this system is self-limiting, and activity will cease when lithospheric strength is sufficient to resist external forces and support isostatic imbalances. A simple force-balance model demonstrates that the force required to uplift the axial zone is tectonically reasonable and that the system can subsequently withstand significant tensional forces. This example shows that crust-mantle boundary uplift coupled with reduced crustal heat production can profoundly affect the long-term strength of the continental lithosphere and may be a critical process in the tectonic stabilization of intraplate regions.

Citation: Aitken, A. R. A., P. G. Betts, R. F. Weinberg, and D. Gray (2009), Constrained potential field modeling of the crustal architecture of the Musgrave Province in central Australia: Evidence for lithospheric strengthening due to crust-mantle boundary uplift, *J. Geophys. Res.*, *114*, B12405, doi:10.1029/2008JB006194.

1. Introduction

[2] Compared to plate margin orogens, compressional intraplate orogens are relatively rare in the geological record and as a result the lithospheric processes occurring in these orogens are poorly understood. Two remarkable examples are preserved in central Australia: the Devonian to Carboniferous Alice Springs Orogeny, which reworked the Paleoproterozoic Arunta Inlier [*Biermeier et al.*, 2003; *Sandiford*, 2002] and the late Neoproterozoic to early Cambrian Petermann Orogeny, which reworked the Mesoproterozoic Musgrave Province [*Camacho et al.*, 1997; *Camacho and Fanning*, 1995; *Maboko et al.*, 1991, 1992; *Scrimgeour and Close*, 1999].

[1]School of Geosciences, Monash University, Melbourne, Victoria, Australia.

[2]Minerals, Petroleum and Energy Group, Primary Industries and Resources South Australia, Adelaide, South Australia, Australia.

0148-0227/09/2008JB006194$09.00

[3] Each of these intraplate orogens was the last tectonic event to have pervasively affected its host terrane [*Collins and Shaw*, 1995; *Edgoose et al.*, 2004; *Major and Conor*, 1993], and crustal scale deformation during these events is therefore interpreted to be the dominant control on the crustal architecture of central Australia [*Camacho and McDougall*, 2000; *Goleby et al.*, 1990; *Lambeck*, 1983; *Lambeck and Burgess*, 1992]. The Arunta Inlier and the Musgrave Province (Figure 1) are associated with high amplitude (150 mGal) relative Bouguer gravity highs, each 100 km wide, within a subcircular gravity low that covers most of central Australia (Figure 1) possibly representing a region of thick continental crust [*Clitheroe et al.*, 2000; *Shaw et al.*, 1995; *Wellman*, 1988]. Isostatic analyses of central Australia have shown that at the wavelength of these regional gravity anomalies (~200 km) central Australia cannot be isostatically compensated using a conventional isostatic model [*Kirby and Swain*, 2006; *Stephenson and Lambeck*, 1985]. This indicates that the continental lithosphere in this region is locally strong enough to sustain short-wavelength (200 km) isostatic disequilibrium, although these loads may be collectively

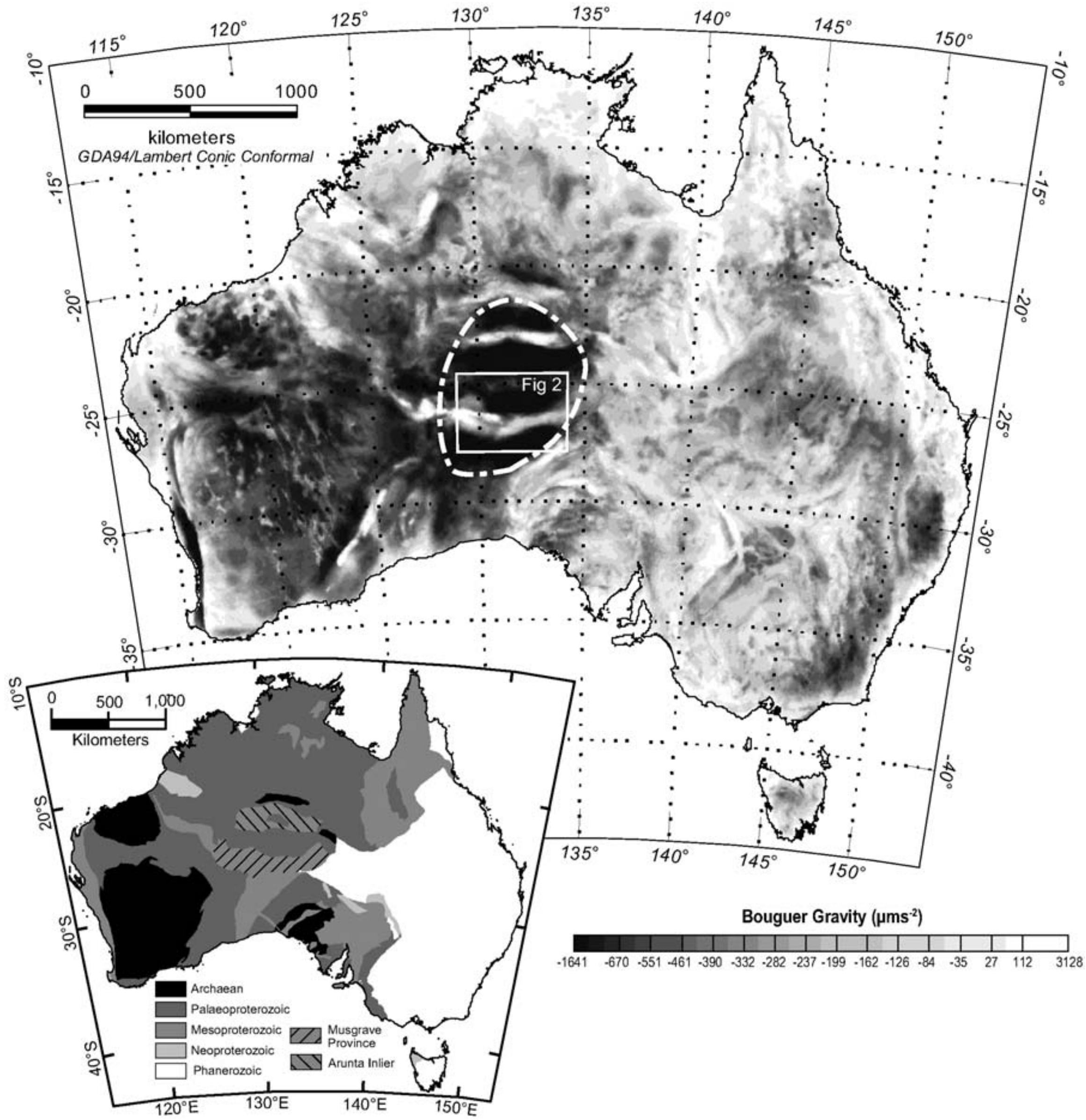

Figure 1. A map of gridded Bouguer gravity anomalies within Australia, and their relation to the major crustal elements (after *Shaw et al.*, 1995). The Musgrave and Arunta provinces are associated with prominent east–west trending relative highs within the central Australian gravity low (dot-dashed white line). Gravity grid used under license from Geoscience Australia.

supported by long-wavelength (1000 km) lithospheric flexure, causing the regional gravity low (Figure 1).

[4] Seismic and gravity data over the Arunta Inlier have provided a reasonable degree of constraint on the crustal architecture of this province and have demonstrated that the crust-mantle boundary is uplifted by $\sim$25 km along the lithospheric scale Redbank Thrust Zone, and that this offset is sufficient to cause the relative gravity high [*Goleby et al.*, 1989, 1990; *Korsch et al.*, 1998]. A similar but less well constrained model derived from teleseismic data over the Musgrave Province proposes up to 30 km of crust-mantle boundary uplift, occurring along steep lithospheric scale reverse shear zones during the Petermann Orogeny [*Lambeck and Burgess*, 1992; *Lambeck et al.*, 1988].

[5] These crust-mantle boundary offsets have apparently been preserved for several hundred million years despite significant forces resulting from isostatic disequilibrium [*Lambeck and Burgess*, 1992] and a number of tectonic events of large magnitude elsewhere in the continent during the Phanerozoic [*Betts et al.*, 2002] including the Lachlan Orogeny [e.g., *Gray and Foster*, 2004] and Gondwana Breakup [e.g., *Cande and Mutter*, 1982; *Veevers*, 1990]. Such long-lived stability implies high integrated lithospheric strength. This is inconsistent with the relative weakness required to focus intraplate strain during intraplate orogenesis [*Braun and Shaw*, 2001; *Hand and Sandiford*, 1999; *Sandiford*, 2002; *Sandiford and Hand*, 1998; *Sandiford et al.*, 2001], suggesting that lithospheric processes occurring

during orogenesis have led to a significant increase in the integrated lithospheric strength of these regions.

[6] New gravity profiles across the Musgrave Province, collected with a data spacing of approximately 1 km [*Gray and Aitken*, 2007; *Gray et al.*, 2007; *Gray and Flintoft*, 2006] provide an opportunity to produce more detailed models of its crustal architecture. We present petrophysically constrained, two-dimensional forward models along these gravity profiles to test the likelihood of a crust-mantle boundary offset, and better define its magnitude and geometry. We also explore the geodynamic system of the Petermann Orogeny, with a focus on defining the mechanism by which the integrated lithospheric strength of the region was increased sufficiently to permit the preservation of a significant crust-mantle boundary offset for hundreds of millions of years.

2. Geological Setting of the Petermann Orogeny

[7] The Musgrave Province preserves a variety of gneissic rocks of dominantly felsic lithology with precursors dated ~1600 Ma. [e.g., *Gray*, 1978; *Wade et al.*, 2006] that were metamorphosed at amphibolite to granulite facies during the ~1200 Ma, Musgravian Orogeny [e.g., *Camacho and Fanning*, 1995; *Gray*, 1978; *Maboko et al.*, 1991; *Sun and Sheraton*, 1992; *White et al.*, 1999]. The emplacement of the charnockites and granites of the Pitjantjatjara Supersuite at ~1190–1150 Ma occurred during and shortly after this orogeny [*Camacho and Fanning*, 1995; *Edgoose et al.*, 2004; *Major and Conor*, 1993; *White et al.*, 1999] and their emplacement pattern, along with a structural grain within basement gneiss, defines the northeast trending architecture of the Musgravian Orogeny in aeromagnetic data [*Aitken and Betts*, 2008]. Subsequent to the Musgravian Orogeny, the voluminous mafic intrusions of the Giles Complex and coeval dykes were emplaced within the Musgrave Province during the extensional Giles Event, at ~1080 Ma [*Clarke et al.*, 1995b; *Glikson et al.*, 1995; *Sun et al.*, 1996] along with surficial volcanic rocks now exposed at the margins of the Musgrave Province [*Glikson et al.*, 1995]. A further extensional event ~800 Ma was characterized by a continent-scale southeast oriented dyke swarm and the inception of the Officer and Amadeus Basins [*Zhao et al.*, 1994]. These basins are commonly interpreted as part of the once contiguous Centralian Superbasin [*Walter et al.*, 1995].

[8] The crustal architecture resulting from these events was then reworked during the ~570–530 Ma Petermann Orogeny, which occurred under N–S compression in an intraplate setting [*Aitken and Betts*, 2009; *Camacho et al.*, 1997; *Maboko et al.*, 1992; *Scrimgeour and Close*, 1999]. This orogeny was characterized by the development of crustal scale shear zones at high pressures and relatively low temperatures and a lack of magmatism [*Edgoose et al.*, 2004; *Wade et al.*, 2008]. Outcropping Petermann Orogeny shear zones are typically oblique reverse mylonite, ultramylonite and pseudotachylite zones, varying from a few meters in width to several kilometers [*Clarke et al.*, 1995a; *Edgoose et al.*, 2004], and in aeromagnetic data they are characterized by linear, narrow and strongly negative magnetic anomalies representing magnetite depleted crustal scale shear zones [*Aitken and Betts*, 2008, 2009; *Aitken et al.*, 2008]. Large regions where pre-Petermann Orogeny structure is well preserved throughout the Musgrave Province indicate that strain during the Petermann Orogeny was highly partitioned onto these crustal scale shear zones [*Aitken et al.*, 2008; *Camacho and McDougall*, 2000; *Edgoose et al.*, 2004].

[9] The most fundamental shear zone at the surface is the late Neoproterozoic to early Cambrian (570–530 Ma) Woodroffe Thrust [*Camacho and Fanning*, 1995; *Maboko et al.*, 1992] which is a shallowly south-dipping mylonite zone up to 3 km wide [*Edgoose et al.*, 2004], and has a strike length of greater than 500 km (Figure 2). The Woodroffe Thrust is interpreted to have accommodated north-directed thrusting of the granulite facies Fregon Subdomain over the amphibolite facies Mulga Park Subdomain which are interpreted as differing crustal levels of the same terrane [*Camacho and Fanning*, 1995; *Maboko et al.*, 1992]. Further shear zones of similar scale also outcrop in the northern Fregon Subdomain, including the Mann Fault, the Ferdinand Fault and the Hinckley Fault [*Major and Conor*, 1993]. These shear zones are matched further south by the aeromagnetically defined Wintiginna Lineament and Lindsay Lineament [*Major and Conor*, 1993], which are of comparable scale to the Mann Fault and Woodroffe Thrust (Figure 2).

[10] The exact timing and duration of deformation during the Petermann Orogeny is uncertain, with the limited geochronology available being too imprecise to define a well-constrained evolution. Studies of deposition in the Officer Basin adjacent to the Musgrave Province, have indicated that deposition of sediments derived from the Musgrave Province started ~600 Ma [*Wade et al.*, 2005] and continued in episodic pulses until ~500 Ma [*Haddad et al.*, 2001].

[11] Geochronological constraints on the Petermann Orogeny from within the orogen are largely derived from metamorphic assemblages. The earliest radiometric ages derived for the Petermann Orogeny are observed near the northern margin of the province, in the vicinity of the Piltardi Detachment Zone (Figure 2). This region is interpreted to represent folding of both crystalline basement and the overlying sedimentary rocks into a series of nappes above an upper crustal decollement. [*Flottmann et al.*, 2005; *Scrimgeour et al.*, 1999]. Rb-Sr on biotite in granite yielded ages of 600 and 560 Ma [*Forman*, 1972; *Scrimgeour et al.*, 1999] and K-Ar on muscovite in the Dean Quartzite yielded ages of 586 ± 5 Ma [*Scrimgeour et al.*, 1999].

[12] Studies of the metamorphic history of the Fregon Subdomain in the Musgrave Ranges and Tomkinson Ranges (Figure 2) have identified prograde subeclogite facies metamorphism and retrograde amphibolite facies to greenschist facies metamorphism in Petermann Orogeny shear zones [*Camacho et al.*, 1997; *Clarke et al.*, 1995a; *Ellis and Maboko*, 1992; *Maboko et al.*, 1991]. These metamorphic events were also recognized in studies of the Mann Ranges (Figure 2), however in this region migmatitic shear zones at high metamorphic grade were also identified as an intermediate phase of deformation between the subeclogite and amphibolite facies events [*Edgoose et al.*, 2004; *Scrimgeour and Close*, 1999; *Scrimgeour et al.*, 1999].

[13] Radiometric dating of these metamorphic events is sparse and poorly constrained, however, Sm-Nd dating on recrystallized dykes indicated that subeclogite facies

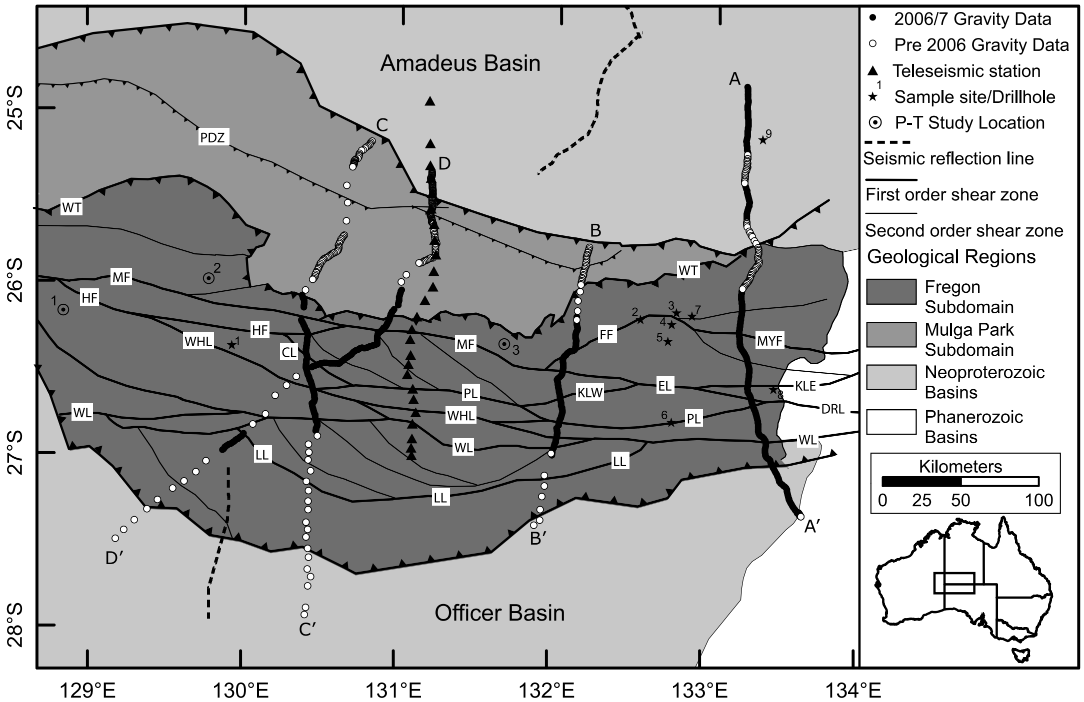

Figure 2. Map of the Musgrave Province showing the locations of gravity stations used in modeling, teleseismic stations, P-T study areas (1, Tomkinson Ranges; 2, Mann Ranges; 3, Musgrave Ranges), deep seismic reflection profiles, and petrophysical sample/drillhole locations (1, Deering Hills; 2, FPD1; 3, KP1/KP2; 4, MID1; 5, WHD1; 6, WW1/WW3; 7, K2D3/K2D5; 8, DU2; 9, Erldunda 1). The locations of major shear zones delineated from magnetic data are shown following the nomenclature outlined by *Major and Conor* [1993] where possible, with new names defined for others: WT, Woodroffe Thrust; MF, Mann Fault; HF, Hinckley Fault; CL, Caroline Lineament (new name); FF, Ferdinand Fault; MYF, Marryat Fault; EL, Echo Lineament; KLW, Kaltjiti Lineament West (new name); KLE, Kaltjiti Lineament East (new name); PL, Paroora Lineament; DRL, De Rose Lineament;WHL, Wintiginna-Hinckley Lineament (new name); WL, Wintiginna Lineament; LL, Lindsay Lineament; PDZ, Piltardi Detachment Zone.

(~12 kbar, ~650°C) mylonitization occurred at 547 ± 30 Ma in the Musgrave Ranges [*Camacho et al.*, 1997; *Ellis and Maboko*, 1992], while high-pressure garnet granulite facies (9.2 kbar, 730°C) assemblages were Sm-Nd dated at 494 ± 59 Ma north of the Mann Ranges [*Scrimgeour et al.*, 1999]. The subeclogite facies (14 ± 1 kbar, 700–750°C) shear zones in the Tomkinson Ranges have not been radiometrically dated [*Clarke et al.*, 1995a].

[14] The migmatitic shear zones in the Mann Ranges have been dated using U-Pb SHRIMP on zircon and K-Ar on hornblende, yielding ages of 561 ± 11 and 565 ± 9 Ma, respectively [*Scrimgeour et al.*, 1999], placing an upper age limit on the undated retrograde amphibolite facies shear zones (7 ± 2 kbar, 660 ± 50°C) [*Scrimgeour and Close*, 1999]. Greenschist facies (~4 kbar, 400°C) [*Maboko et al.*, 1991] shear zones in the Musgrave Ranges return metamorphic ages clustered within 540 ± 10 Ma [*Camacho et al.*, 1997; *Camacho and Fanning*, 1995; *Camacho and McDougall*, 2000; *Maboko et al.*, 1991, 1992].

[15] The metamorphic evolution suggested by these data, and the preservation of minerals with low closure temperatures that yield ages older than 800 Ma proximal to ~550 Ma eclogite facies shear zones [*Camacho et al.*, 2001] has been interpreted to indicate that the Fregon Subdomain was buried to lower crustal depth early in the Petermann Orogeny, but was uplifted to upper crustal depth shortly afterward [*Camacho et al.*, 1997]. This formed the basis of a geodynamic model derived from P-T data that proposed crustal thickening in the early stages of the Petermann Orogeny, before exhumation began, progressing to a crustal scale positive flower structure [*Camacho and McDougall*, 2000].

[16] In addition to these metamorphic studies in the axial zone of the province, the mineralogy of the Giles Complex and associated rocks defines sharp transitions in the exposed crustal level related to major shear zones. A southward shallowing in the emplacement depth is represented by a transition from ultramafic plutons emplaced at ~6 kBar [*Clarke et al.*, 1995a], through gabbro-pyroxenite, troctolite, and finally surficial volcanic rocks [*Glikson et al.*, 1995, 1996]. This indicates that since ~1080 Ma, the axial zone of the province has been uplifted by approximately 20 km relative to the margins of the province.

[17] On the basis of its metamorphic history, the axial zone of the Musgrave Province has been largely unaffected by later events, although epidote-quartz alteration in some shear zones in the eastern Musgrave Province has been interpreted to represent reworking of the Musgrave Province during the Alice Springs Orogeny [*Edgoose et al.*, 1993; *Young et al.*, 2002]. In contrast, the southern margin of the

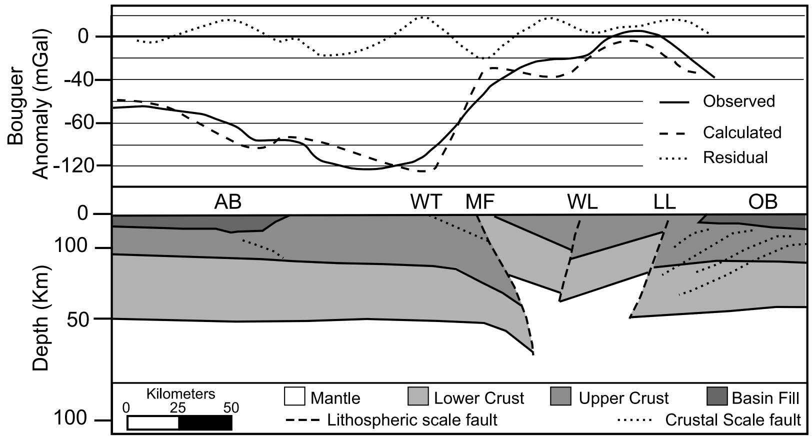

Figure 3. The model of deep crustal architecture derived from teleseismic data, also showing the fit to gravity data, modified from *Lambeck and Burgess* [1992] and *Korsch et al.* [1998]. Shear zone abbreviations are as in Figure 2. OB, Officer Basin; AB, Amadeus Basin.

Musgrave Province and the adjacent Officer Basin have each experienced significant tectonism and subsidence during the Delamerian and Alice Springs Orogenies [*Haddad et al.*, 2001; *Lindsay*, 2002]. Although its effects were somewhat localized to the eastern Officer Basin, the Delamerian Orogeny is associated with thrust faulting, both within the basin sequence [*Hoskins and Lemon*, 1995], and at its margin with the Musgrave Province [*Lindsay and Leven*, 1996], and several hundred meters of subsidence [*Haddad et al.*, 2001]. Again, subsidence during the Alice Springs Orogeny has only been recognized in the eastern Officer Basin [*Haddad et al.*, 2001; *Lindsay*, 2002], however seismic reflection data further west (Figure 2) has imaged a major thrust complex at the southern margin of the Musgrave Province that has deformed the Ordovician to Devonian strata of the Officer Basin, suggesting activity during the ~450–320 Ma Alice Springs Orogeny [*Lindsay and Leven*, 1996].

[18] Tectonism subsequent to the Alice Springs Orogeny is not recognized in the stratigraphy or structuring of the Officer Basin, however the thermal history of the eastern Officer Basin may suggest several subsequent kilometer-scale erosion events [*Tingate and Duddy*, 2002]. Although these erosional events are likely to have also affected the Musgrave Province, its crustal architecture has almost certainly been preserved since at least the late Paleozoic, and probably the early Cambrian. This is despite large isostatic stress differences of up to 80 MPa [*Lambeck and Burgess*, 1992], and multiple phases of extension and shortening related to the evolution of Phanerozoic Australia at the eastern margin of the plate [*Betts et al.*, 2002; *Gray and Foster*, 2004], and net extension during Gondwana breakup [*Betts et al.*, 2002].

3. Crustal Architecture of the Musgrave Province

[19] Current knowledge of the crustal architecture of the Musgrave Province at depth is based on a single teleseismic transect across the province [*Lambeck and Burgess*, 1992; *Lambeck et al.*, 1988], supplemented by deep seismic reflection data in the Amadeus Basin [*Korsch et al.*, 1998] and at the southern margin of the Musgrave Province [*Lindsay and Leven*, 1996] (Figure 2). The model based on teleseismic data (Figure 3) is characterized by steep Moho penetrating shear zones, corresponding to the Mann Fault, Wintiginna Lineament and Lindsay Lineament, that accommodate an upward Moho offset of up to 30 km beneath the central Musgrave Province [*Lambeck and Burgess*, 1992]. Due to the inherent uncertainty in passive seismic data [e.g., *Fishwick and Reading*, 2008; *McQueen and Lambeck*, 1996], this model is equivocal, and although a reasonable fit to the regional Bouguer gravity anomaly is achieved, a series of shorter wavelength (<50 km) residual anomalies of about 20 mGal remain (Figure 3), indicating that the crustal density distribution is far from resolved in this model.

[20] Joint modeling of a combination of closely sampled gravity and aeromagnetic data, with constraints from petrophysical measurements permits a high confidence model of the structure and density distribution of the near surface [e.g., *Farquharson et al.*, 2008; *Fullagar et al.*, 2008; *McLean and Betts*, 2003] and therefore improves the constraint on deep crustal architecture. In 2005, gravity coverage in the Musgrave Province was generally at an average data spacing of 7.5 to 10 km, and did not allow the effective separation of near-surface and deep density anomalies: a data collection program was therefore undertaken.

3.1. High-Resolution Gravity Surveys in the Musgrave Province

[21] The gravity data collection program acquired 643 gravity measurements at approximately 1 km spacing along four gravity profiles traversing the regional gravity anomaly in the eastern and central Musgrave Province (Figure 2). Gravity measurements were made with a Scintrex CG-5 gravimeter, with 3D location data determined relative to the Australian Height Datum using a Sokkia GSR 2600 RTK differential GPS system; data accuracy is estimated at 0.05 mGal, based on the accuracy of repeat measurements and the GPS error. Given the regional nature of the survey and the flatness of the terrain in this region terrain corrections were deemed unnecessary, however, care was taken to avoid localized topography (e.g., creeks and sand dunes). Survey methods are described in detail by *Gray and Flintoft* [2006], *Gray and Aitken* [2007], and *Gray et al.* [2007]. Access to the Musgrave Province is subject to cultural

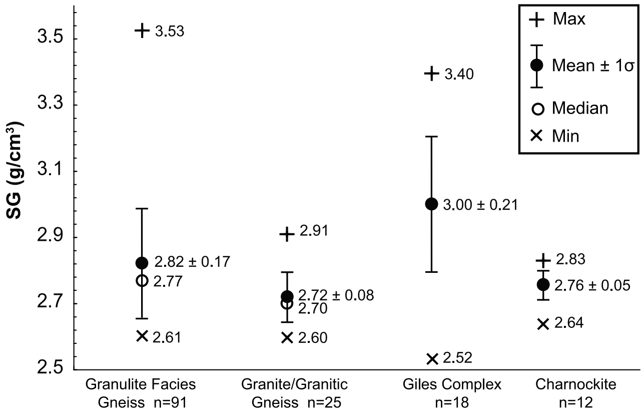

Figure 4. Chart showing the maximum, minimum, and mean with 1 standard deviation (σ) of density data collected throughout the Musgrave Province, divided into broad lithological groups. The median density is also shown where it does not equal the mean density.

restrictions, and off-road access is severely restricted. As a result, the gravity profiles are incompletely sampled, with the exception of the Stuart Highway profile (profile A). To fill in gaps and to extend the model profiles, the new data were supplemented by older data, which, although often sparse, merge well with the new data.

3.2. Petrophysics Data

[22] Although cultural access restrictions limited surface sampling to a single area in the Deering Hills, drillcore was available covering a larger area throughout the Fregon Subdomain (Figure 2). Specific gravity measurements from these sites were collated into Data Set S1 in which they were subdivided by lithology into granulite facies gneiss (the Birksgate Complex), granitic gneiss/granites, and charnockites (both Pitjantjatjara Supersuite), and Giles Complex mafic rocks (Figure 4).[1]

[23] The rocks of the Musgrave Province are dominantly layered gneisses and granulites within which specific gravity varies markedly on the decameter scale. Thus our specific gravity measurements, collected from hand samples and drillcore, cannot be directly linked to the density of large model cells, with volumes of several cubic kilometers. The statistical distributions of these density measurements are however representative of the overall density of the near-surface rocks. The median density of granulite facies gneiss incorporating both mafic and felsic samples, 2770 kgm^{-3}, was used to constrain the density value of the granulite facies crust in forward modeling (Figure 5). Because of the large standard deviation (Figure 4), sensitivity analysis was undertaken to quantify the effect that this parameter has on the forward models (Figure 6).

3.3. Joint Two-Dimensional Forward Modeling of Gravity and Magnetic Data

[24] The profiles were jointly modeled with magnetic and free air gravity data using the profile based 2D modeling software GM-sys, which is based on the methods of *Talwani* [1965], *Talwani et al.* [1959], and *Talwani and Heirtzler* [1964], and uses the algorithm of *Won and Bevis* [1987]. This forward-modeling software represents geological bodies as 2D polygons of arbitrary shape and density, for which the gravity response is computed, assuming infinite extent in the third dimension [*Talwani et al.*, 1959]. The topography obtained from the gravity readings was maintained in modeling and free air gravity was calculated at this surface for each measurement. Reduced to pole magnetic field was calculated for an elevation 80 m above the topographic surface for stations every 500 m. An arbitrary DC shift was automatically applied to the calculated gravity and magnetic anomaly curves to provide the lowest misfit to the observed data.

[25] Regional aeromagnetic data over the Musgrave Province, were collected with north–south lines at 400 m spacing, east–west tie lines at 4000 m spacing and a draped nominal flying height of 80 m. These data, reduced to pole, were used to constrain the shallow geometry of structures along each profile (Figures 5a, 5d, 5g, and 5j). The major lithologies in the Musgrave Province have distinct magnetic signatures [*Aitken and Betts*, 2009; *Aitken et al.*, 2008] and can be reliably identified in aeromagnetic data. High magnetic contrast is observed between Petermann Orogeny shear zones and the granitic and gneissic basement, permitting magnetic modeling of the shallow geometry of shear zones (Figure 5). Most Giles Complex and Pitjantjatjara Supersuite plutons are also magnetically distinct, and their locations and geometry were also defined (Figure 5). These shallow magnetic models were constrained by outcropping geology and also satisfy the short-wavelength component of high-resolution gravity data where it is available.

[26] For gravity modeling of the crustal scale architecture, a three-layered crust was inferred from seismic data [*Korsch et al.*, 1998] with intracrustal boundaries at 15 and 30 km depth and the crust-mantle boundary at 50 km depth [*Clitheroe et al.*, 2000; *Korsch et al.*, 1998]. The lower crustal layers and mantle were assumed to be laterally homogenous, with densities of 2850, 3100 and 3300 kgm^{-3}, respectively, and the upper crust was subdivided into large blocks representing the granulite facies crust of the northern Fregon Subdomain, the amphibolite facies crust of the Mulga Park Subdomain and the southern Fregon Subdomain, and also the Officer and Amadeus Basins. In accordance with the petrophysical data (Figure 4), granulite facies crust was assigned a median density of 2770 kgm^{-3}, Pitjantjatjara Supersuite intrusions were assigned either a density of 2760 kgm^{-3}, where charnockitic, or 2720 kgm^{-3} where granitic, and Giles Complex intrusions were assigned a density of 3000 kgm^{-3} No petrophysical data were available for the amphibolite facies crust in the Mulga Park Subdomain or the southern Fregon Subdomain and so these regions are not directly constrained, however the high-resolution gravity data indicates a density contrast of about 100 kgm^{-3} across the Woodroffe Thrust, and amphibolite facies blocks were assigned a median density of 2670 kgm^{-3}. Although the seismic reflection data do not match up with any of our gravity profiles (Figure 2) the geometry of the Amadeus and Officer Basins was extrapolated from these onto our profiles. This geometry was further constrained by joint gravity and magnetic modeling of shallow structure and on profile A, the Erldunda No 1 Borehole, approximately 35 km along the

[1]Auxiliary materials are available at ftp://ftp.agu.org/apend/jb/2008jb006194.

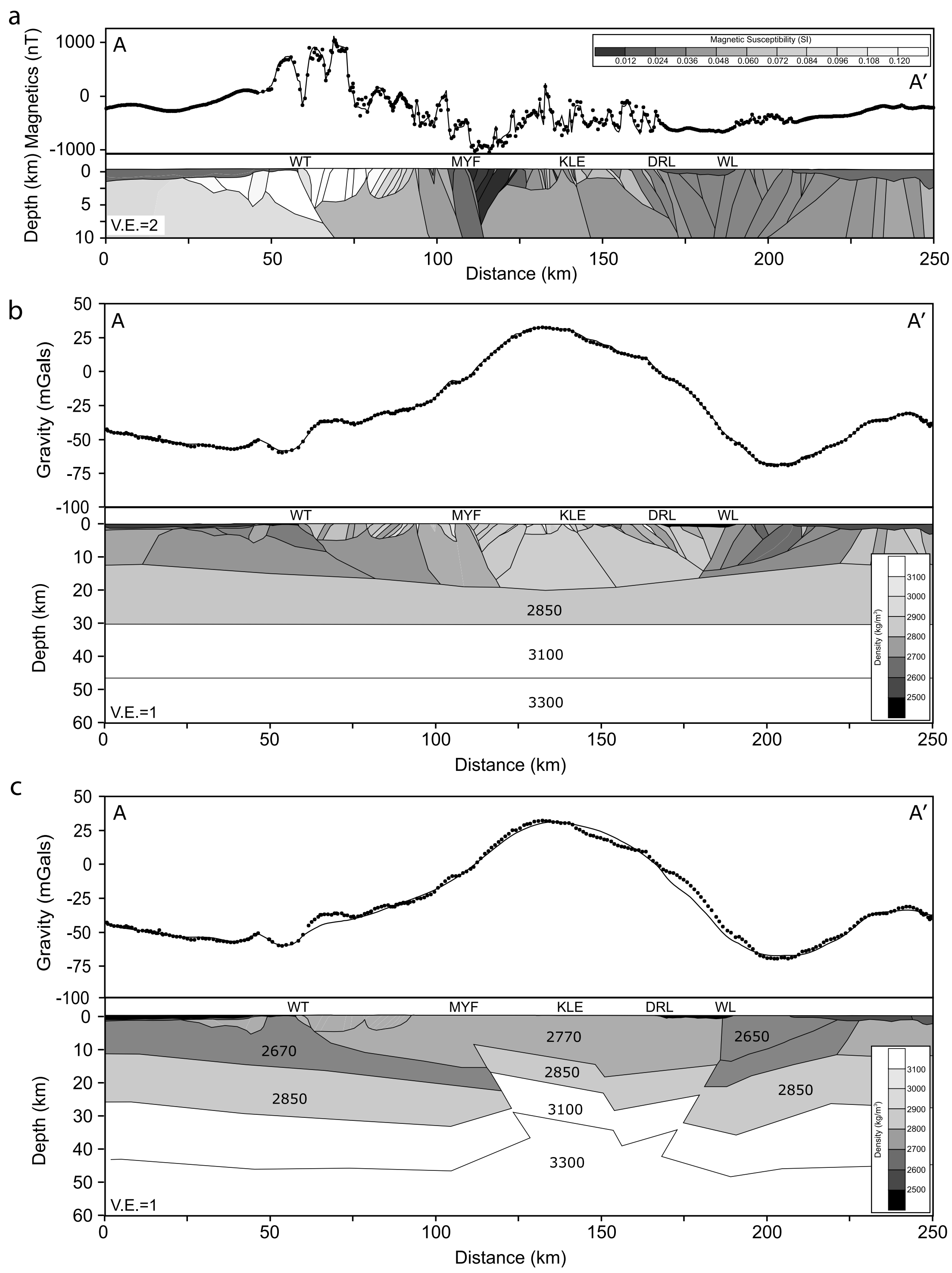

Figure 5. Experimental model development for each of the four profiles: (a, d, g, and j) Shallow crustal architecture defined by magnetic modeling, note vertical exaggeration of two. (b, e, h, and k) Midcrustal decollement models. (c, f, i, and l) Median density models. Shaded block densities are denoted by the scale bar, and annotated values in kgm^{-3}. Shear zone abbreviations are as in Figure 2.

profile (Figures 2 and 7a–7c). A density of 2550 kgm^{-3} was assumed for the Amadeus and Officer Basins, with the exception of the Bitter Springs Formation on profile A, with a density of 2600 kgm^{-3}.

[27] From this basic starting model, several models were produced. A midcrustal decollement is a common feature of compressional orogens [e.g., *Ziegler et al.*, 1998] and this possibility was investigated in a model with a heterogeneous upper crust above a flat and laterally homogenous lower crust and mantle. These crustal decollement models (Figures 5b, 5e, 5h, and 5k) show that for each profile the regional gravity anomaly can be explained by an upper

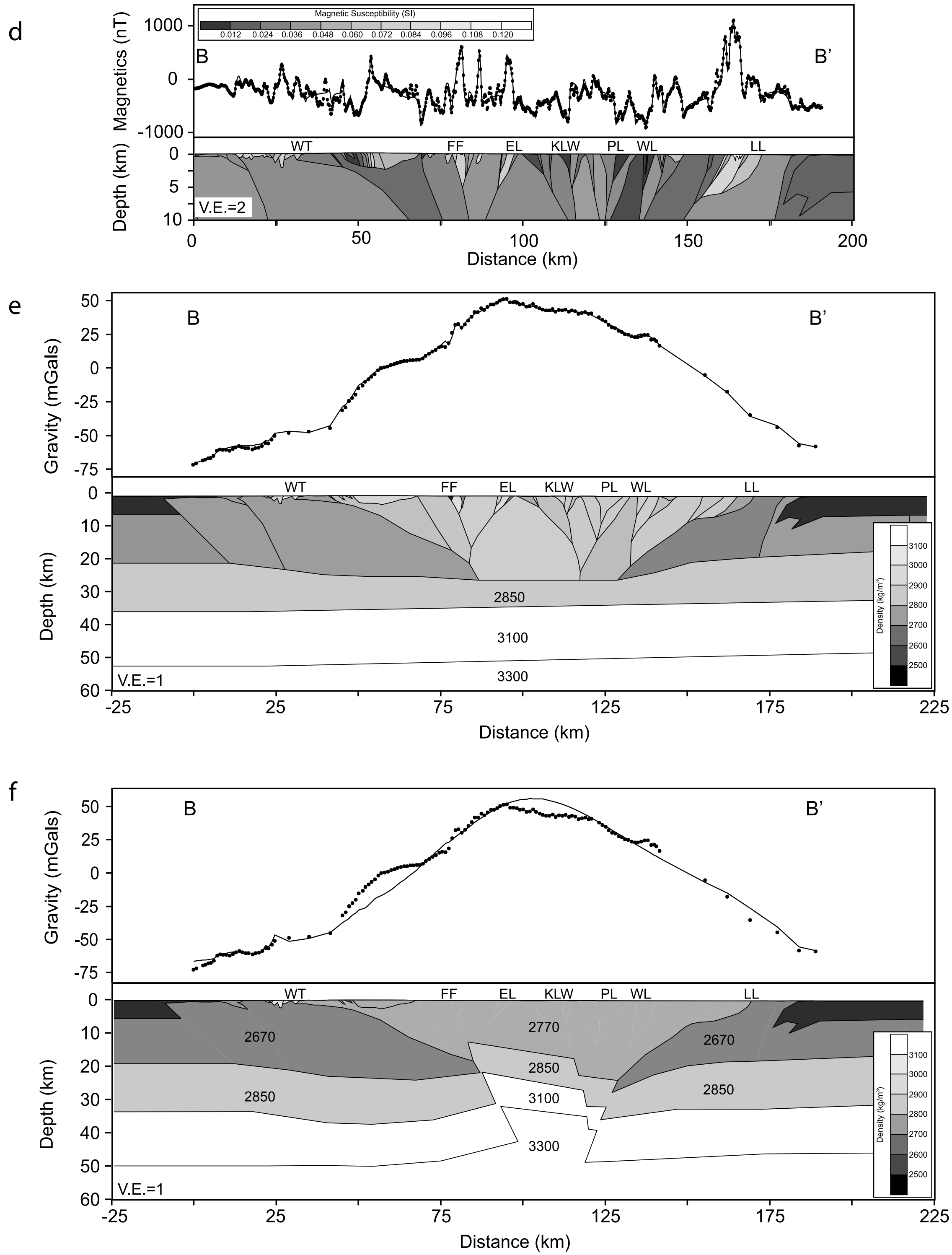

Figure 5. (continued)

crustal density distribution alone and that there is no intrinsic requirement in the gravity data for crust-mantle boundary offset. However, the density distribution required to satisfy the gravity anomaly is inconsistent with the petrophysical data collected, as it requires large regions within the granulite facies gneiss with densities either in excess of 2850 kgm^{-3} or less than 2700 kgm^{-3}, and equally large regions with densities less than 2650 kgm^{-3} within the amphibolite facies gneiss.

[28] The steepest long-wavelength gradients in the gravity field occur above major shear zones in the interior of the granulite facies Fregon Subdomain (Figure 5), and do not correspond to the surface boundaries that demarcate the transition from amphibolite facies to granulite facies gneiss

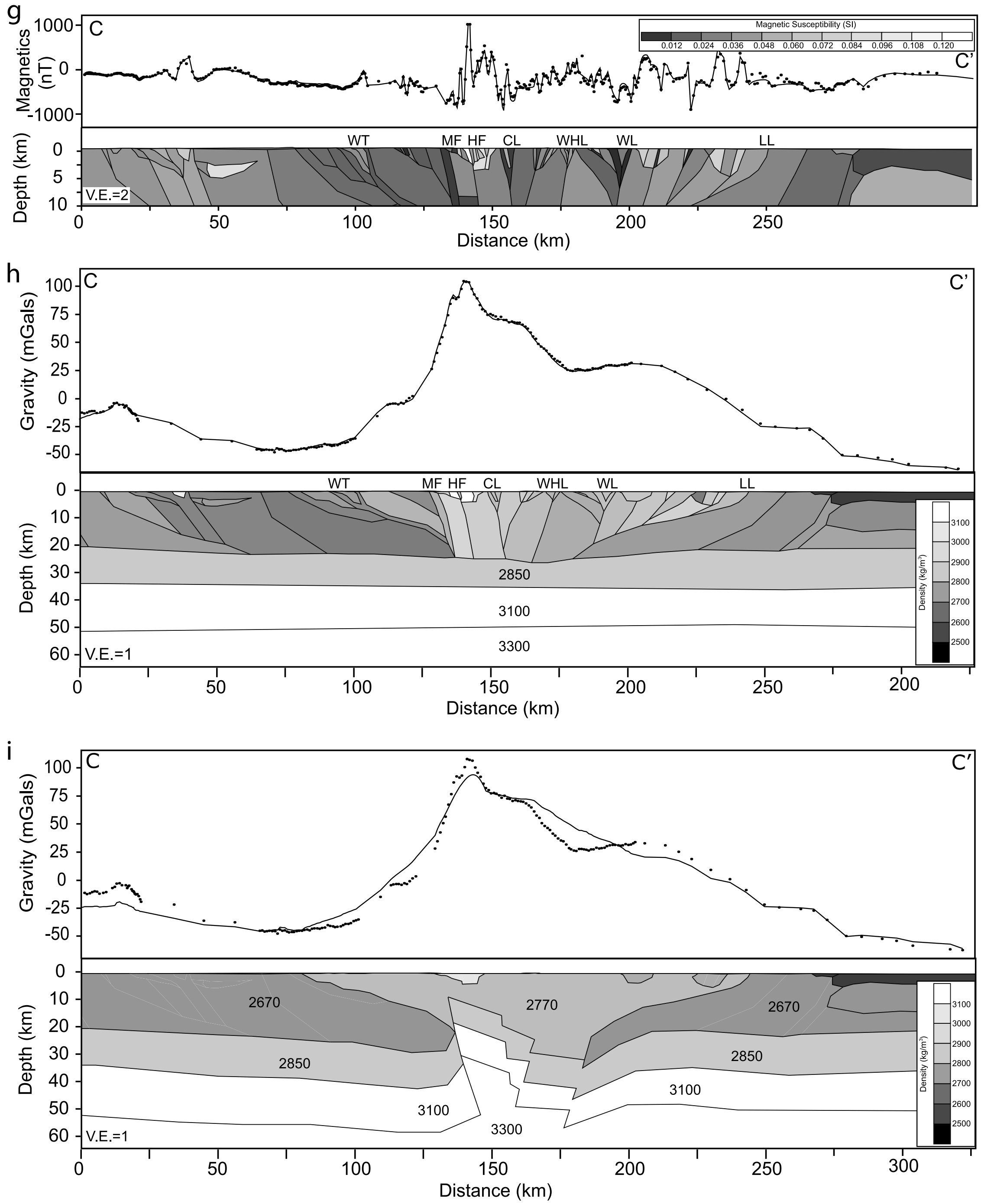

Figure 5. (continued)

(Figure 2). A regional component of the gravity anomaly from crust-mantle boundary relief can explain these long-wavelength gradients, and satisfy the regional anomaly with a more realistic upper crustal density distribution. Median density models were therefore constructed to define the most probable geometry of the deeper crustal layers (Figures 5c, 5f, 5i, and 5l). In these median density models, the densities of all blocks were held invariant, and the boundaries between these blocks were modified. To model the lower crust and mantle, the trace of major shear zones at depth was projected from their shallow geometry, and offsets on these fault planes were modeled until the regional anomaly was best satisfied.

[29] These models have resolved the long-wavelength component of the gravity data reasonably well, and indicate 15 to 20 km of crust-mantle boundary offset on the Mann Fault, Ferdinand Fault and Marryat Fault, and 10 to 15 km of crust-mantle boundary offset on the Wintiginna and Wintiginna Hinckley Lineaments. These offsets define an uplifted wedge of lithospheric mantle beneath the axial zone of the province (Figure 5).

[30] The density contrast between granulite facies crust and amphibolite facies crust contributes significantly to the regional gravity anomaly, and thus small variations in this parameter will affect the deeper model geometry. The

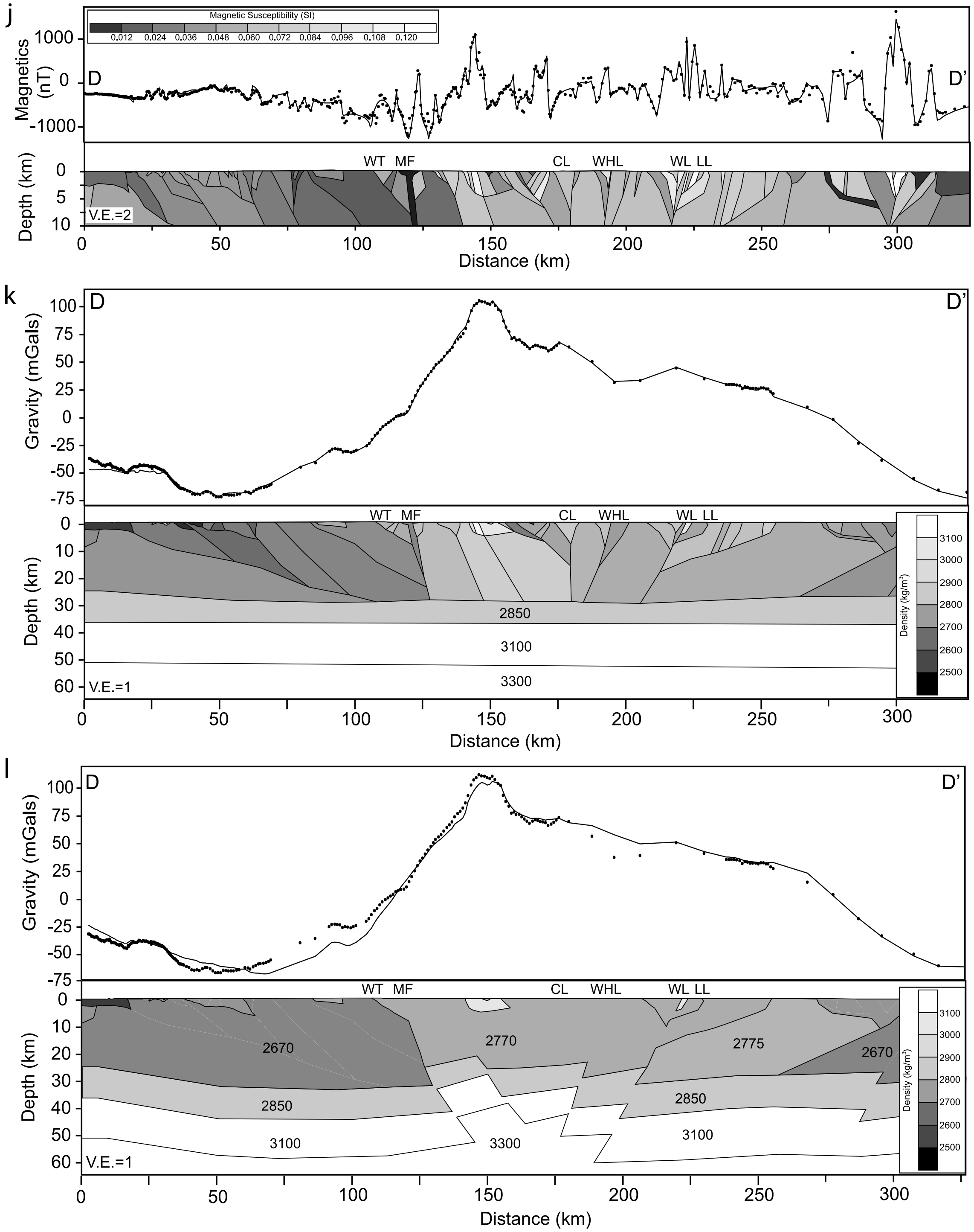

Figure 5. (continued)

sensitivity of the deeper geometry on profiles A and C was analyzed for density contrasts up to 70 kgm^{-3} above and below the median density model (Figures 6a and 6b). This analysis showed that a fit to the regional anomaly can be achieved with a density contrast between 30 kgm^{-3} and 140 kgm^{-3}, although these upper and lower values do not fit the short-wavelength gravity gradient across the Woodroffe Thrust. This analysis also demonstrates that the crustal architecture in the vicinity of the Mann Fault and beneath the Woodroffe Thrust is relatively insensitive to this parameter, but that the crustal architecture in the vicinity of the Wintiginna Lineament and beneath the Lindsay Lineament is much more sensitive to this parameter.

[31] In constructing the median density models, the Mann Fault and Wintiginna Lineament were assumed to be planar, with the near-surface dip valid at depth. The sensitivity of the model geometry to the dip of these shear zones was tested by imposing dips of between 80° and 40° on these planar shear zones. For profile A, a fit to the data was possible for dips between 70° and 50°, within which the

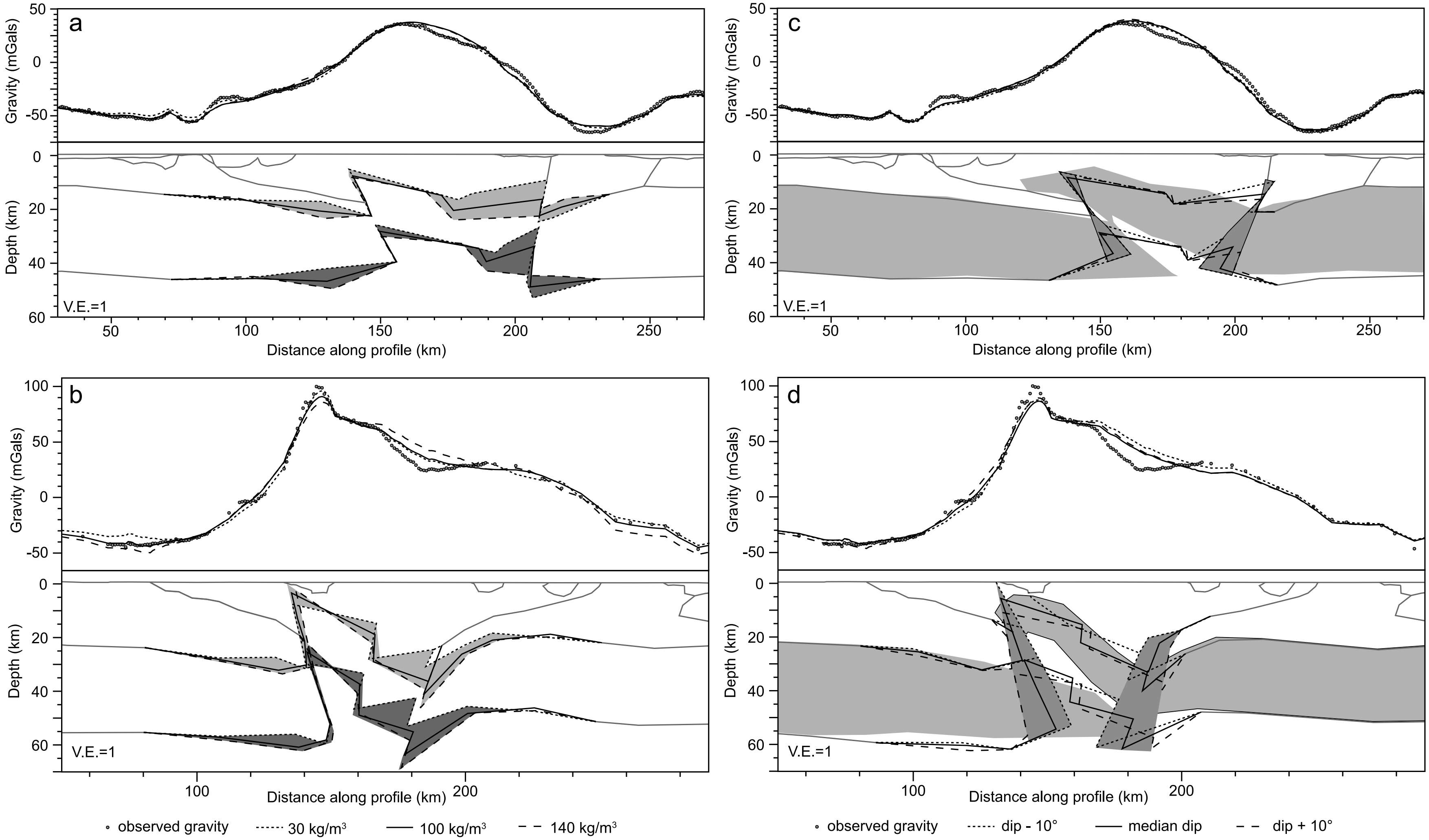

Figure 6. (a) The sensitivity of the crust-mantle boundary geometry of profile A to variations in the density contrast between granulite facies crust and amphibolite facies crust. (b) The density sensitivity analysis for profile C, and (c) sensitivity of the crust-mantle boundary geometry of profile A to the dip of major shear zones. Dark-shaded areas indicate the region of sensitivity with dips between 50° and 70°. The light-shaded area indicates the lower crustal geometry required with 40° dip. (d) The dip sensitivity analysis for profile C; in this case the dark-shaded area indicates dips between 60° and 80°, and the light-shaded area indicates the lower crustal geometry required with 40° dip.

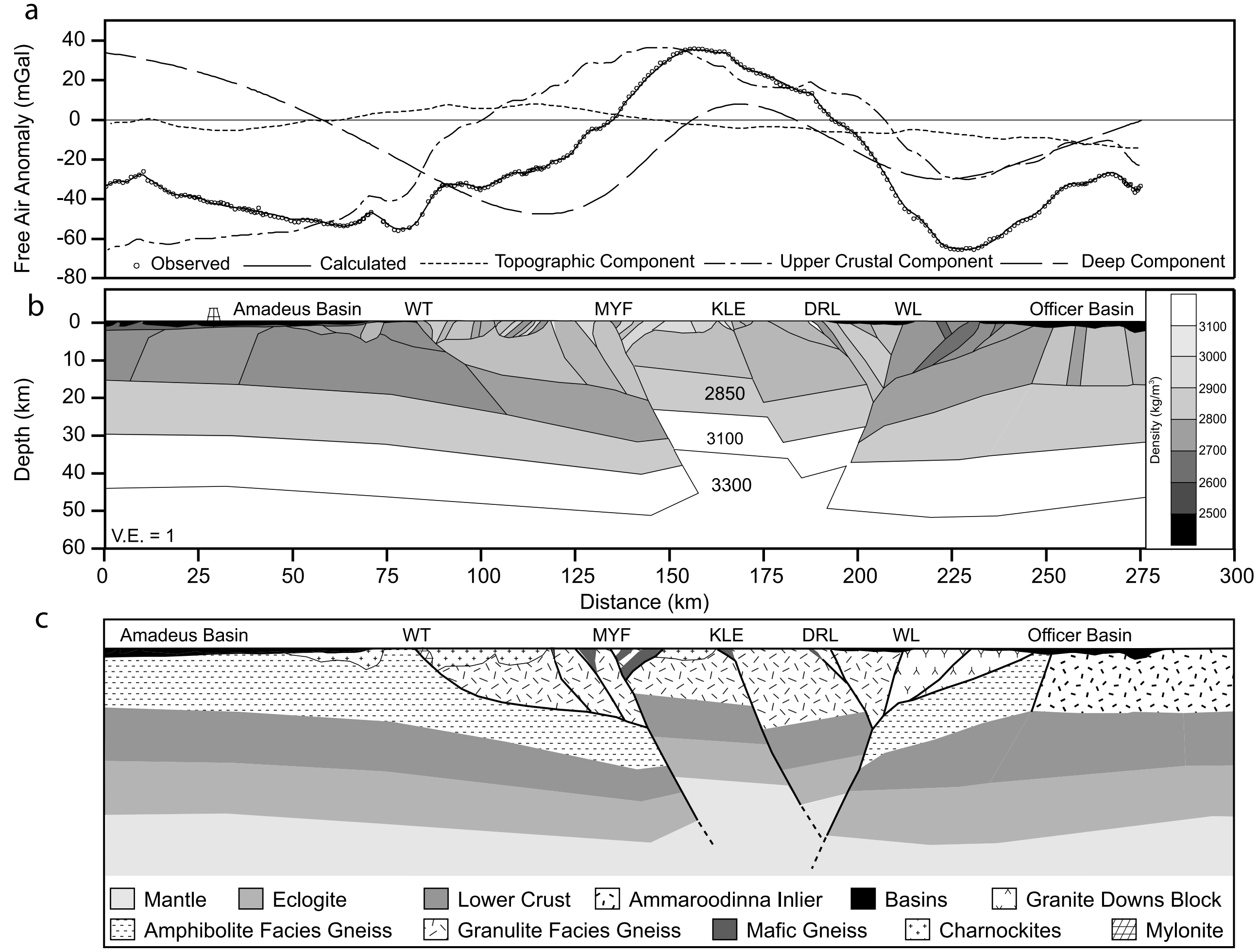

Figure 7. Our best fitting models for each profile: (a, d, g, and j) Observed and calculated free air anomalies, also showing the components of the calculated anomaly from topography (dotted line), the upper crustal density distribution (dot-dashed line), and the lower crust/upper mantle geometry (long-dashed line). (b, e, h, and k) The density distribution that produces the calculated anomaly in Figures 7a, 7d, 7g, and 7j. (c, f, i, and l) Schematic model, showing the major structures and lithologies. Shaded block densities are denoted by the scale bar, and annotated values in kgm^{-3}. Shear zone abbreviations are as in Figure 2.

geometry varies little (Figure 6c). Profile C is similar, with a fit to the data possible for dips between 80° and 60°, again with little variation in the geometry (Figure 6d).

[32] For shallower dips, 40° or less, a fit to the gravity data is only possible by invoking extreme uplift (>35 km) and nappe style folding of the lower crust and crust-mantle boundary above the Woodroffe Thrust (Figures 6c and 6d). While this geometry cannot be absolutely excluded on the basis of our gravity models, we consider smaller offsets on steeper faults to be more probable. A similar conclusion was reached by *Lambeck and Burgess* [1992] who showed that offset along a shallow dipping Woodroffe Thrust cannot explain the teleseismic data.

3.4. Most Probable Models of the Crustal Architecture of the Musgrave Province

[33] The preceding models (Figure 5) demonstrate that a crust-mantle boundary offset of 15 to 20 km is highly probable, but cannot completely explain the gravity anomaly. Incorporating a variable upper crust into the median density models results in a good gravity data misfit, but perhaps more importantly does not require densities that differ significantly from the median densities, except in localized areas. These most probable models (Figure 7) show a characteristic crustal architecture with an axial zone of steep, lithospheric scale shear zones that bound granulite facies blocks of different crustal levels, flanked by much shallower reverse shear zones that accommodated the thrusting of granulite facies gneiss over amphibolite facies gneiss.

[34] The regional gravity low over the amphibolite facies Mulga Park Subdomain is caused by a combination of low to moderate upper crust density, and a crust-mantle boundary depression of up to 10 km. The Woodroffe Thrust is defined in the gravity data by a gravity low which is interpreted to be due to a 2–3 km wide low-density mylonite zone, but there is also a short-wavelength step across the Woodroffe Thrust, indicating the juxtaposition of the low to moderate density Mulga Park Subdomain to the high density Fregon Subdomain. Our models indicate that the crustal scale Woodroffe Thrust is shallowly south dipping, and links into the litho-

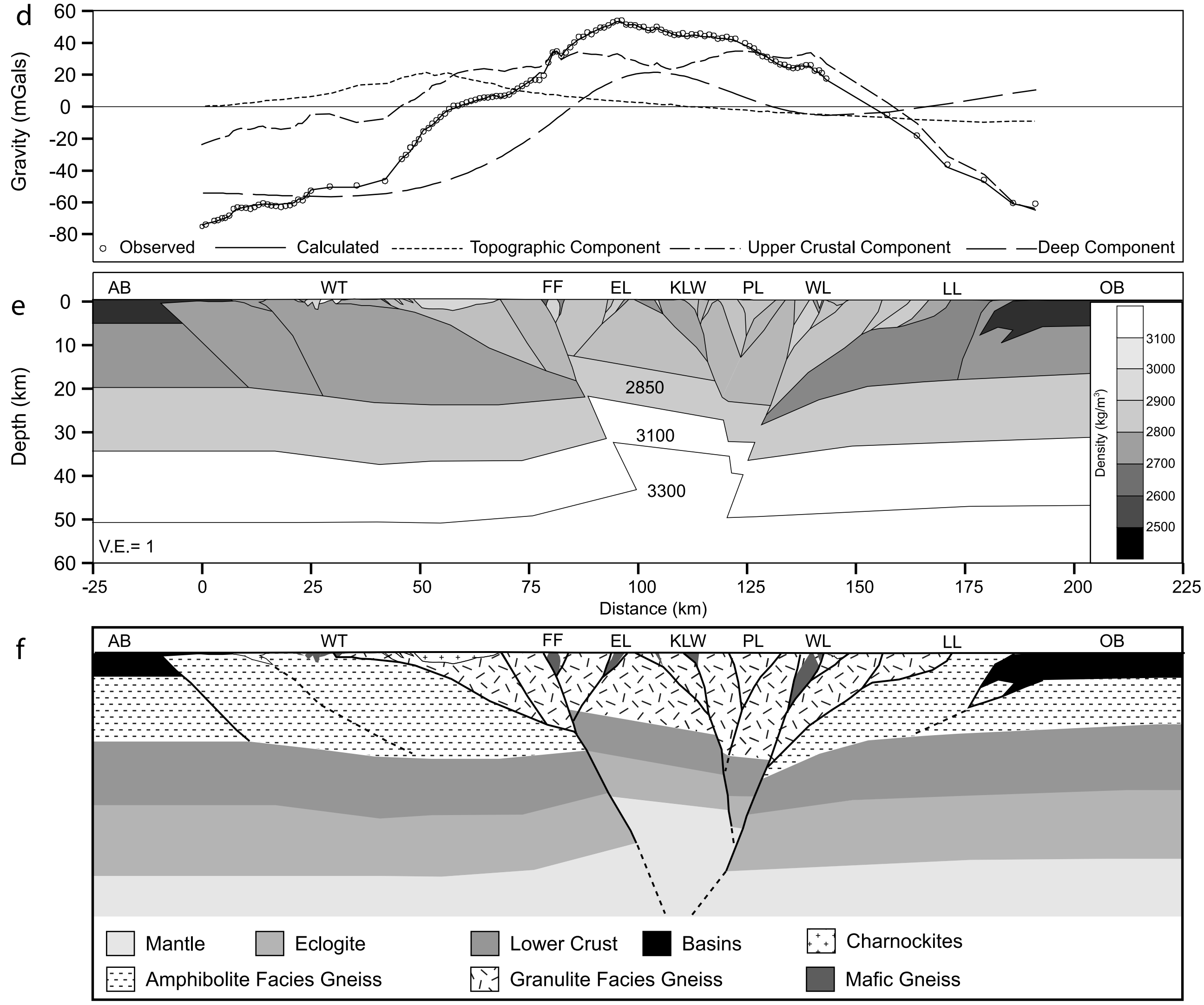

Figure 7. (continued)

spheric scale Mann-Ferdinand-Marryat fault system at a depth of approximately 20 km.

[35] Although it is the major metamorphic grade boundary and near-surface density boundary, the Woodroffe Thrust does not correspond to the principal regional gravity gradient, which lies to the south over the Mann Fault (Figures 7g–7l), Ferdinand Fault (Figures 7d–7f) and Marryat Fault (Figures 7a–7c). In contrast to the Woodroffe Thrust, the short-wavelength gravity signal across these shear zones reflects only the density of the shear zone, and the density contrast between blocks on either side is small. This implies that the regional gravity gradient is due to a deep seated source. Our modeling indicates that this steep regional gradient can be attributed to south block up vertical offset on these crustal scale shear zones, displacing the crust-mantle boundary by between 10 and 20 km along the lithospheric scale Mann-Ferdinand-Marryat fault system, and causing the uplift of dense mantle material into the lower crust.

[36] The dense crustal blocks south of the Mann-Ferdinand-Marryat fault system contain charnockite and Giles Complex mafic intrusions and are dissected by several southeast and east trending shear zones, several of which (e.g., the Caroline Lineament, the Hinckley Fault) may be of sufficient scale to cause crust-mantle boundary offset.

[37] The moderately to steeply south-dipping Kaltjiti Lineament (Figures 7a–7f) and the more steeply north-dipping Wintiginna-Hinckley Lineament (Figures 7g–7l) are associated with both short- and long-wavelength gravity gradients. Our model indicates a sharp reduction in near-surface density as a result of a southward increase in exposed crustal level, associated with approximately 10 km of north block up vertical offset on these shear zones. This implies a normal shear sense on the south-dipping Kaltjiti Lineament, and a reverse shear sense on the north-dipping Wintiginna-Hinckley Lineament. A similar combination of short- and long-wavelength anomalies across the steeply north dipping Wintiginna Lineament indicates the juxtaposition of blocks from different crustal levels due to approximately 10 km of north block up vertical offset on this shear zone.

[38] South of the Wintiginna Lineament, crust-mantle boundary offset is not supported by the gravity data. The near-surface density structure south of the Wintiginna Lineament is not consistent along strike: In the far eastern

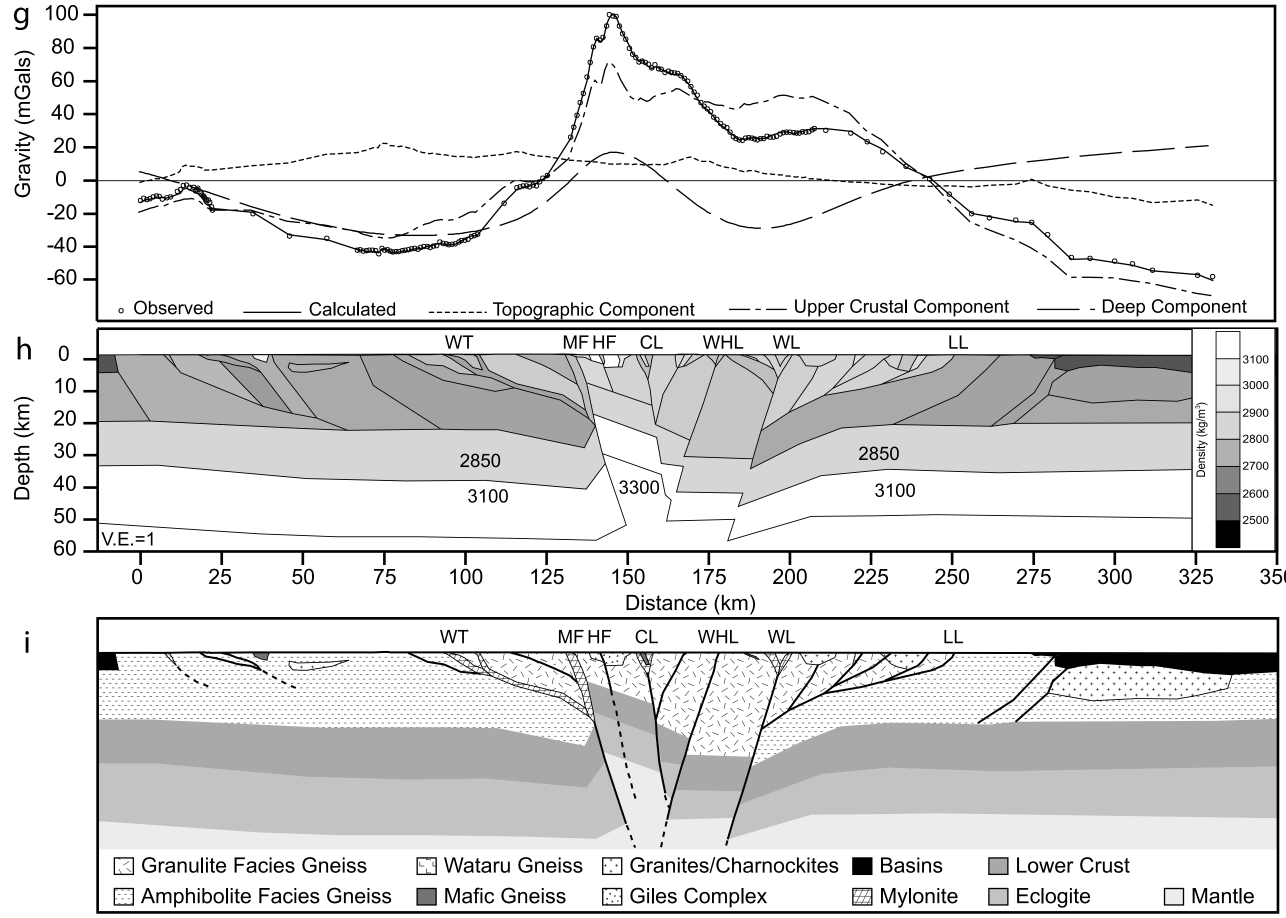

Figure 7. (continued)

Musgrave Province (Figures 7a–7c) the low-density (2650 kgm^{-3}) Granite Downs block represents a transition from granulite to amphibolite facies crust across the Wintiginna Lineament. In the eastern and central Musgrave Province (Figures 7d–7i) our modeling indicates dense blocks (2800 kgm^{-3}) above a moderately to shallowly dipping Lindsay Lineament with less dense (2670 kgm^{-3}) crust below. In the western-central Musgrave Province (Figures 7j–7l) high gravity values persist beyond the Lindsay Lineament, over the granulite facies Wataru Gneiss, until low-density (2700 kgm^{-3}) Pitjantjatjara Supersuite granites and amphibolite facies crust are observed at the province margin and beneath the Officer Basin.

[39] In summary, our gravity modeling indicates that the Woodroffe Thrust and Lindsay Lineament are shallow-dipping crustal scale thrust faults that link to steeper transpressional shear zones at a depth of approximately 20 km. These first-order shear zones, the Mann-Ferdinand-Marryat fault system and the Wintiginna Lineament, delineate the boundaries of an axial zone of anastomosing transpressional shear zones. The east trending regional gravity high is associated with this zone, and our petrophysically constrained modeling indicates that it is due to between 10 and 20 km of crust-mantle boundary offset along these shear zones, causing a wedge of lithospheric mantle to be emplaced within the lower crust, rather than high densities in the near surface.

[40] At depth, this crustal architecture is similar to that proposed from seismic models (Figure 3) with the exception that neither the Lindsay Lineament nor the southern province marginal thrust penetrate the crust-mantle boundary, as suggested previously [*Korsch et al.*, 1998; *Lambeck and Burgess*, 1992]. Crust-mantle boundary uplift south of the Wintiginna Lineament is not supported, because a relatively thin wedge of granulite facies gneiss above a shallow dipping Lindsay Lineament is sufficient to satisfy the gravity anomaly here.

3.5. Structure of the Lithospheric Mantle Beneath the Musgrave Province

[41] A recent continent-scale seismic tomography model has identified a positive velocity gradient in the upper mantle beneath central Australia, which was interpreted to represent either a region of relatively hot lithospheric mantle, or a region of different composition to the surrounding material [*Fishwick and Reading*, 2008]. This model cannot, however, resolve features at the scale of the Musgrave Province, and in the absence of lithospheric scale seismic reflection or magnetotelluric studies, the structure of the lithospheric mantle beneath the Musgrave Province is not known.

[42] The geometry of the crust-mantle boundary is, however, imaged in the gravity models, and this allows an estimate of the amount of shortening in the upper mantle,

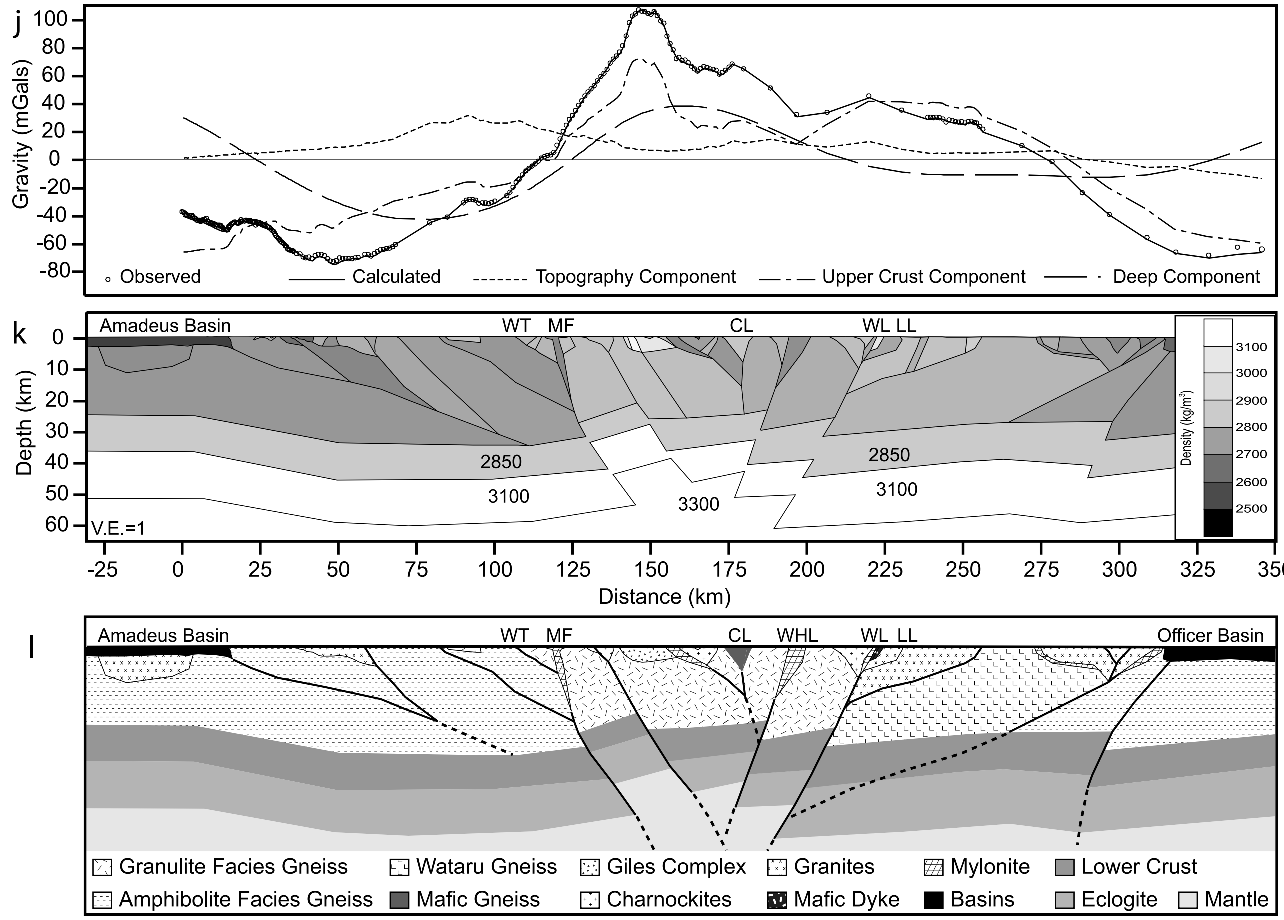

Figure 7. (continued)

from which the amount of mantle lithosphere thickening can be estimated. Reconstructing a flat crust-mantle boundary from our models (Figure 7) yields total north–south shortening within the Musgrave Province of between 4 and 6%. The depth to the base of the lithospheric mantle is unknown beneath the Musgrave Province, and the amount of lithospheric thickening is estimated by assuming that shortening was accommodated by downward cylindrical buckling of the mantle lithosphere, which is independent of lithospheric thickness. Lithospheric thickening is estimated at approximately 35 km beneath the axial zone of the orogen (Figure 8b). The volume per unit length of this lithospheric root (6000 km^3/m) is considerably greater than the volume per unit length of the uplifted wedge of mantle (500 km^3/m), suggesting net thickening of the lithospheric mantle during the Petermann Orogeny (Figure 8c), unless counteracted by delamination of the lithospheric root beneath the orogen.

4. A Kinematic Model of the Petermann Orogeny

[43] Any geodynamic model proposed for the Petermann Orogeny must address the three principal characteristics of this orogeny: (1) the localization of strain in this 200 km wide region, distant from plate boundaries; (2) lithospheric thickening, followed by the uplift of the entire crustal pile by ~15–20 km; and (3) local strengthening of the lithosphere during the orogeny such that this region has been able to sustain isostatic disequilibrium for hundreds of millions of years.

4.1. Strain Localization

[44] The present crustal architecture of the Musgrave Province is not a reliable indicator of the crustal architecture prior to the Petermann Orogeny, and therefore cannot readily be used to examine the localization of strain to the Musgrave Province. Strain localization processes for intraplate orogenesis are primarily understood from thermal and thermomechanical models, several of which are relevant to the Petermann Orogeny. Thermal blanketing of the lithosphere by sedimentation has been shown to result in a significant reduction in lithospheric strength by heating of the entire crust [*Karner*, 1991; *Lavier and Steckler*, 1997]. This effect is enhanced where the upper crust is rich in heat producing elements, which, on the basis of high surface heat flow, is interpreted to be the case in much of central Australia [*Cull*, 1982; *McLaren et al.*, 2005; *Scrimgeour and Close*, 1999]. Thermal blanketing of an upper crust rich in heat producing elements by the Centralian Superbasin has been proposed to explain the localization of strain during the Petermann Orogeny to the Musgrave Province, where the Centralian Superbasin was interpreted to be thickest [*Hand and Sandiford*, 1999; *Sandiford and Hand*, 1998].

[45] However, this model is speculative and is disputed on the grounds of an emergent Musgrave Province source proposed for detrital zircons in ~700 Ma to ~500 Ma

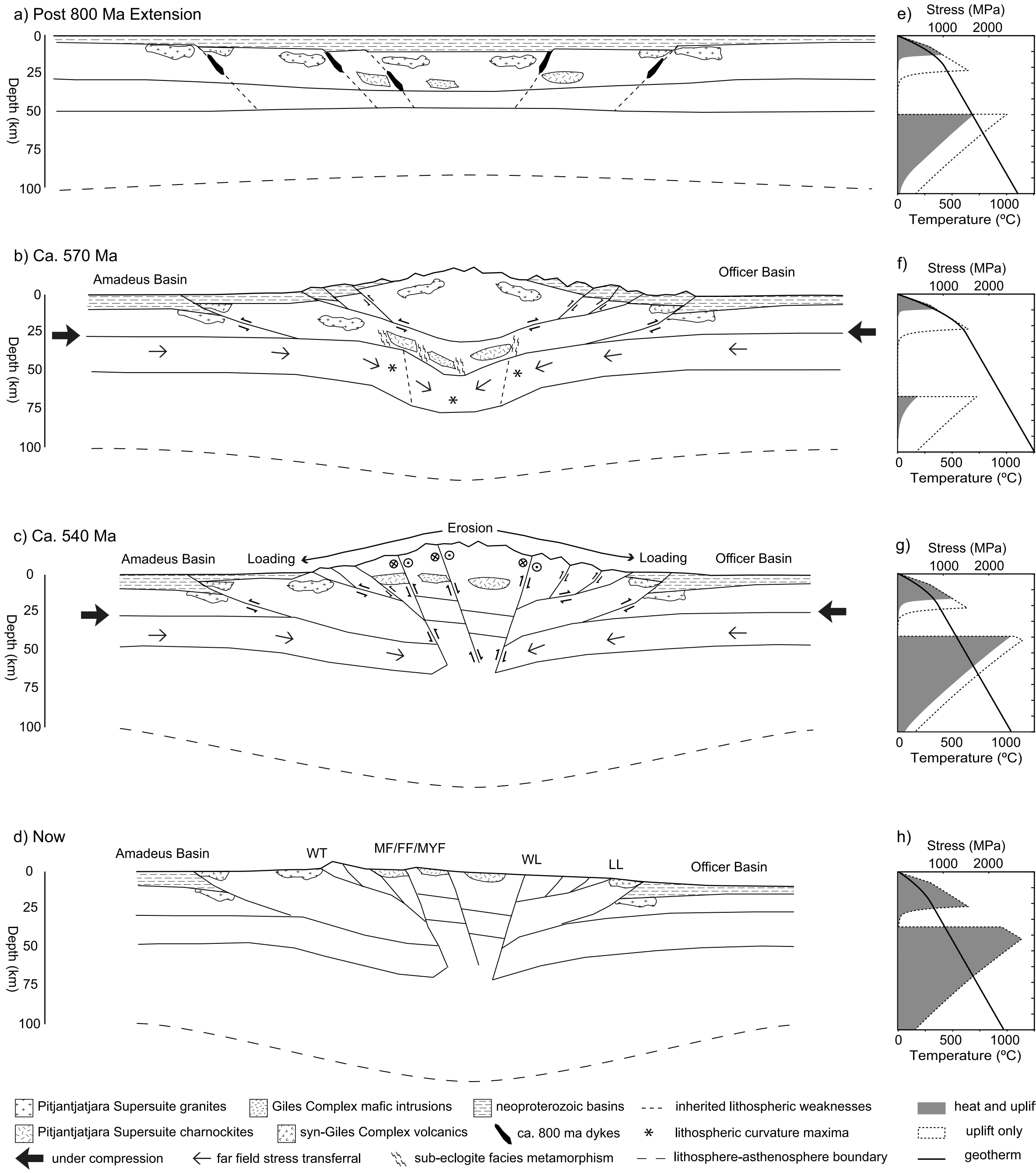

Figure 8. Schematic evolution of the architecture of the Musgrave Province through the Petermann Orogeny and its likely influence on the thermal state of the lithosphere and the integrated lithospheric strength of the region. (a) Relict postextensional architecture, (e) with relatively hot and relatively weak lithosphere (moho temperature, T_m = 683°C; integrated lithospheric strength, $F_i = 4.47 \times 10^{13}$ Nm^{-1}). (b) Lithospheric thickening increased the thickness of the heat producing layer and the crust, and (f) caused heating of the system (T_m = 958°C) and a reduction in the integrated lithospheric strength by a factor of 5.72 ($F_i = 7.82 \times 10^{12}$ Nm^{-1}), that promoted failure of the lithosphere. (c) Uplift of the axial zone, accompanied by erosion of the upper crust, and loading of the marginal regions (g) reduced both the thickness and the heat production of the crust, cooled the system (T_m = 533°C) and increased the integrated lithospheric strength dramatically ($F_i = 8.59 \times 10^{13}$ Nm^{-1}). (d) The presently observed crustal architecture after continued erosion and uplift (h) caused further cooling of the system (T_m = 425°C) and a further increase in the integrated strength of the lithosphere ($F_i = 1.27 \times 10^{14}$ Nm^{-1}). Pitjantjatjara Supersuite granites and charnockites and a Giles Complex intrusion and its volcanic equivalent are shown as approximate markers of crustal level. The form of the lithosphere-asthenosphere boundary is drawn to scale, although its absolute depth is not known. We also show the probable evolution of integrated lithospheric strength under exhumation only, i.e., the thermal state of the lithosphere was constant at postorogenic levels throughout.

Amadeus Basin sedimentary rocks [*Camacho et al.*, 2002]. Several other possibilities exist to explain the localization of strain to this region, including the influence of deformation during previous events, and the focusing of deformation at the boundaries between regions of contrasting strength [*Braun and Shaw*, 2001; *Camacho et al.*, 2002; *Sandiford et al.*, 2001], a heat producing layer in the lithospheric mantle [*Neves et al.*, 2008], and Rayleigh-Taylor instability within the mantle [*Neil and Houseman*, 1999] especially if it is augmented by crustal heat production [*Pysklywec and Beaumont*, 2004]. As a result of these uncertainties, the crustal architecture of the Musgrave Province prior to the Petermann Orogeny and the mechanism of strain localization remain poorly understood.

[46] Our interpreted pre-Petermann Orogeny crustal architecture for central Australia (Figure 8a) is a slightly thinned 50 km thick crust reflecting isostatic equilibrium after crustal sagging at ~800 Ma initiated the development of the Amadeus and Officer basins as part of the once contiguous Centralian Superbasin [*Lindsay*, 2002; *Walter et al.*, 1995; *Zhao et al.*, 1994].

4.2. Lithospheric Thickening and Crustal Uplift

[47] Regardless of the initial crustal architecture, compressional forces in the early stages of the Petermann Orogeny ~600 Ma to 570 Ma (Figure 8b) resulted in crustal thickening by divergent thrust stacking and nappe development above a decollement in the upper crust as indicated by the ~580 Ma Piltardi detachment zone in the Petermann Nappe Complex [*Edgoose et al.*, 2004; *Flottmann et al.*, 2005; *Scrimgeour et al.*, 1999] and also in seismic studies of the Officer Basin [*Lindsay and Leven*, 1996]. Our potential field models of crustal architecture demonstrate crustal thickening at the margins of the province accommodated on shallow crustal scale thrusts (Figure 7). Concurrent thickening of the axial zone of the orogen and also the upper lithospheric mantle is highly probable (Figure 8b).

[48] Crustal thickening is interpreted to have caused burial of midcrustal granulite facies rocks to subeclogite facies depths [*Camacho et al.*, 1997; *Camacho and McDougall*, 2000; *Clarke et al.*, 1995a; *Scrimgeour and Close*, 1999]. Burial and exhumation in the time frame indicated by P-T-t data, less than 40 million years [*Camacho and McDougall*, 2000] requires a mechanism to rapidly switch from crustal thickening to the uplift of the entire crustal pile.

[49] With increasing lithospheric thickening, and increasing lithospheric curvature, bending stresses can accumulate in the lithosphere until the yield strength is exceeded causing failure close to the regions of maximum curvature [*Goetze and Evans*, 1979]. We interpret the location and geometry of the Mann Fault and Wintiginna Lineament to reflect the development or reactivation of lithospheric weaknesses close to the regions of maximum curvature (Figure 8b). The activation of these shear zones may have isolated the axial zone of the orogen from the downward force associated with buckling of the lithosphere in response to far field stress, and initiated uplift (Figure 8c). In addition, lithospheric thickening increases the likelihood of partial delamination of the mantle lithosphere, and this may have applied a significant uplifting force to the axial zone.

[50] Once initiated, uplift of the axial zone by 15 to 20 km was primarily accommodated on transpressional shear zones, although the Woodroffe Thrust and Lindsay Lineament remained active (Figure 8c). Similar to orogens elsewhere, mountain building would have unloaded the hinterland by erosion [e.g., *Avouac and Burov*, 1996; *Beaumont et al.*, 2000; *Burov and Toussaint*, 2007] and unroofing [e.g., *Hodges et al.*, 1998] and loaded the foreland by deposition within the Officer and Amadeus Basins [*Camacho et al.*, 2002; *Haddad et al.*, 2001; *Wade et al.*, 2005]. This feedback further amplifies uplift of the axial zone relative to the marginal zones, and may have become the dominant uplift driver (Figure 8c). The uplift of a wedge of mantle into the crust is a self-limiting process, in which uplift will terminate either when a dynamic balance is reached between the forces driving the uplift and the mass of the uplifted wedge, or when lithospheric strength is sufficient to withstand these forces.

[51] We propose that this combination of mantle uplift and upper crustal erosion led to a long-term increase in the lithospheric strength of the axial zone of the orogen, stabilizing its architecture and permitting its preservation to the present-day (Figure 8d). This is supported by the fact that deformation subsequent to the Petermann Orogeny has been distributed around the margins of the province, indicating that the lithospheric strength of the axial zone is significantly greater than that of the province margins. The episodic uplift of the Officer Basin throughout the Phanerozoic [*Tingate and Duddy*, 2002] may also have affected the Musgrave Province, and caused further erosion, leading to further cooling and strengthening.

5. Discussion

5.1. Constrained Potential Field Models of Deep Crustal Architecture

[52] Constrained modeling of potential field data is an effective method for defining the geometry of bodies in the near surface [e.g., *Farquharson et al.*, 2008; *Fullagar et al.*, 2008; *McLean and Betts*, 2003] but is typically less effective for modeling of deeper crustal architecture. This study shows that by collecting closely spaced gravity data and petrophysical measurements, the density structure of the near surface can be well constrained and the crustal architecture at depth can be derived. Sensitivity analysis shows that, in the case of the Musgrave Province, the crust-mantle boundary geometry is well constrained in the vicinity of the Mann, Ferdinand and Marryat Faults and the Woodroffe Thrust, but less well constrained to the south. In part, this is due to closer spaced gravity data and the concentration of petrophysical measurements in the northern region, but also reflects the higher amplitude anomaly and steeper gradients of the northern gravity edge in comparison to the southern gravity edge.

[53] Our models of the crustal architecture of the Musgrave Province imply that crust-mantle boundary offsets are relatively sharp, occurring on the plane of major shear zones. Due to its depth, however, the gravity signal from the crust-mantle boundary is long wavelength (Figure 7) and the short-wavelength geometry of this boundary cannot be constrained by the gravity field. Our interpretation is supported by geological and aeromagnetic studies which show that the major transpressional shear zones extend linearly for several hundred kilometers, indicating that they

Table 1. Parameters Used in the Brace-Goetze Lithosphere Models[a]

Parameter Symbol	Parameter Description	Parameter Value	Parameter Value Source
	Brittle Failure		
μ_1	coefficient of friction pressure <200 MPa	0.85	1
μ_2	coefficient of friction pressure >200 MPa	0.6	1
ρ_c	crustal density	2750 kgm^{-3}	
ρ_m	mantle density	3300 kgm^{-3}	
	Geotherm Calculation		
k	thermal conductivity	3 $Wm^{-1}K^{-1}$	2
q_m	mantle heat flow	0.025 Wm^{-2}	2
S_c	heat production	2–4 μWm^{-3}	2
t_{rad}	heat producing layer thickness	20–25 km	
	Power Law Creep (Quartz)		
$\dot{\varepsilon}$	strain rate	1.0×10^{-15} s^{-1}	
A_q	preexponent constant	5.0×10^6 $MPa^{-3}s^{-1}$	1
Q_q	activation energy	1.9×10^5 $Jmol^{-1}$	1
n_q	exponent	3	1
	Power Law Creep (Olivine)		
$\dot{\varepsilon}$	strain rate	1.0×10^{-15} s^{-1}	
A_o	preexponent constant	7.0×10^4 $MPa^{-3}s^{-1}$	1
Q_o	activation energy	5.2×10^5 $Jmol^{-1}$	1
n_o	power law exponent	3	1
	Dorn Law Creep (Olivine)		
$\dot{\varepsilon}$	strain rate	1.0×10^{-15} s^{-1}	
Q_d	activation energy	5.4×10^5 $Jmol^{-1}$	1
ε_d	critical strain rate	5.7×10^{11} s^{-1}	1
σ_d	critical stress	8500 MPa	1

[a]Parameter values are derived from the following sources: 1, *Brace and Kohlstedt* [1980]; 2, *Sandiford and McLaren* [2002]. Strain rate was chosen to reflect a moderately slow geological process.

are of sufficient scale to penetrate the crust-mantle boundary, and that strain within the axial zone was highly partitioned onto these shear zones [*Aitken et al.*, 2008; *Camacho et al.*, 1997, 2001; *Edgoose et al.*, 2004].

5.2. Lithospheric Strengthening During the Petermann Orogeny

[54] The greater strength of olivine dominated lithospheric mantle compared with typical quartz or feldspar dominated lower crustal rocks at comparable temperatures has been demonstrated by several studies [e.g., *Goetze and Brace*, 1972; *Kirby and Kronenberg*, 1987; *Kusznir and Karner*, 1985]. Thus, the uplift of the lithospheric mantle into the lower crust can be expected to cause an increase in the integrated lithospheric strength of a region. Moreover, uplift may have simultaneously caused a reduction in crustal heat production, due to the erosion and thinning of a heat-producing element-rich upper crust [*Hand and Sandiford*, 1999; *McLaren et al.*, 2005; *Sandiford*, 1999; *Sandiford and Hand*, 1998; *Sandiford et al.*, 2001]. This would have further increased lithospheric strength in the long-term (~100 m.y.).

[55] To provide an estimate of the amount of lithospheric strengthening that occurred during the Petermann Orogeny, Brace-Goetze lithospheric strength models [*Brace and Kohlstedt*, 1980] were calculated for each of the stages in our model (Figures 8e–8h). Although the limitations of Brace-Goetze lithosphere models are well known [e.g., *Kusznir and Park*, 1984; *Ranalli and Murphy*, 1987; *Regenauer-Lieb et al.*, 2006, 2008], they provide a reasonable first-order estimate of long-term relative changes in the integrated strength of the lithosphere with minimal data [*Regenauer-Lieb et al.*, 2008]. To calculate these lithospheric strength models, a steady state geotherm is assumed and a quartz dominated crust containing a heat producing layer in the upper crust and an olivine dominated mantle are used. The parameters used to produce these models are detailed in Table 1. In the absence of crustal heat production measurements for the Musgrave Province, we constrain the level of heat production in the upper crustal heat producing layer with estimates from the Arunta Inlier, where deep crustal mafic granulites have heat production of <1 μWm^{-3}, middle upper crustal granites have heat production of 3–5 μWm^{-3}, and upper crustal sediments have heat production of 1–2 μWm^{-3} [*Sandiford et al.*, 2001; *Sandiford and McLaren*, 2002].

[56] Using a 50 km thick crust, and a 20 km thick heat producing layer at 4 μWm^{-3} to simulate conditions prior to the Petermann Orogeny (Figure 8a), leads to an integrated lithospheric strength of 4.47×10^{13} Nm^{-1}, (Figure 8e). The thickening of the crust and the heat producing layer to 65 km and 25 km, respectively, simulates the initial stage of crustal thickening (Figure 8b). This crustal thickening leads to significantly weaker lithosphere, with an integrated strength of 7.82×10^{12} Nm^{-1} (Figure 8f). Thus, crustal thickening may have reduced the integrated lithospheric strength by a factor of 5.72. Reduced heat production of 3 μWm^{-3} in a 20 km thick heat producing layer, simulates the effects of erosion of the upper crust during latter stage of the orogeny, which, allied with uplift of the crust-mantle boundary to 40 km depth (Figure 8c), leads to an increase in the integrated strength of the lithosphere to 8.59×10^{13} Nm^{-1}, stronger than before the orogen (Figure 8g). A further reduction in the heat production of the 20 km thick heat producing layer to 2 μWm^{-3}, and further uplift of the crust-mantle boundary to 35 km depth simulates subsequent erosion of the upper crust (Figure 8d), and causes a further increase in the integrated strength of the lithosphere to 1.27×10^{14} Nm^{-1}. Thus, incorporating both the uplift of the mantle into the

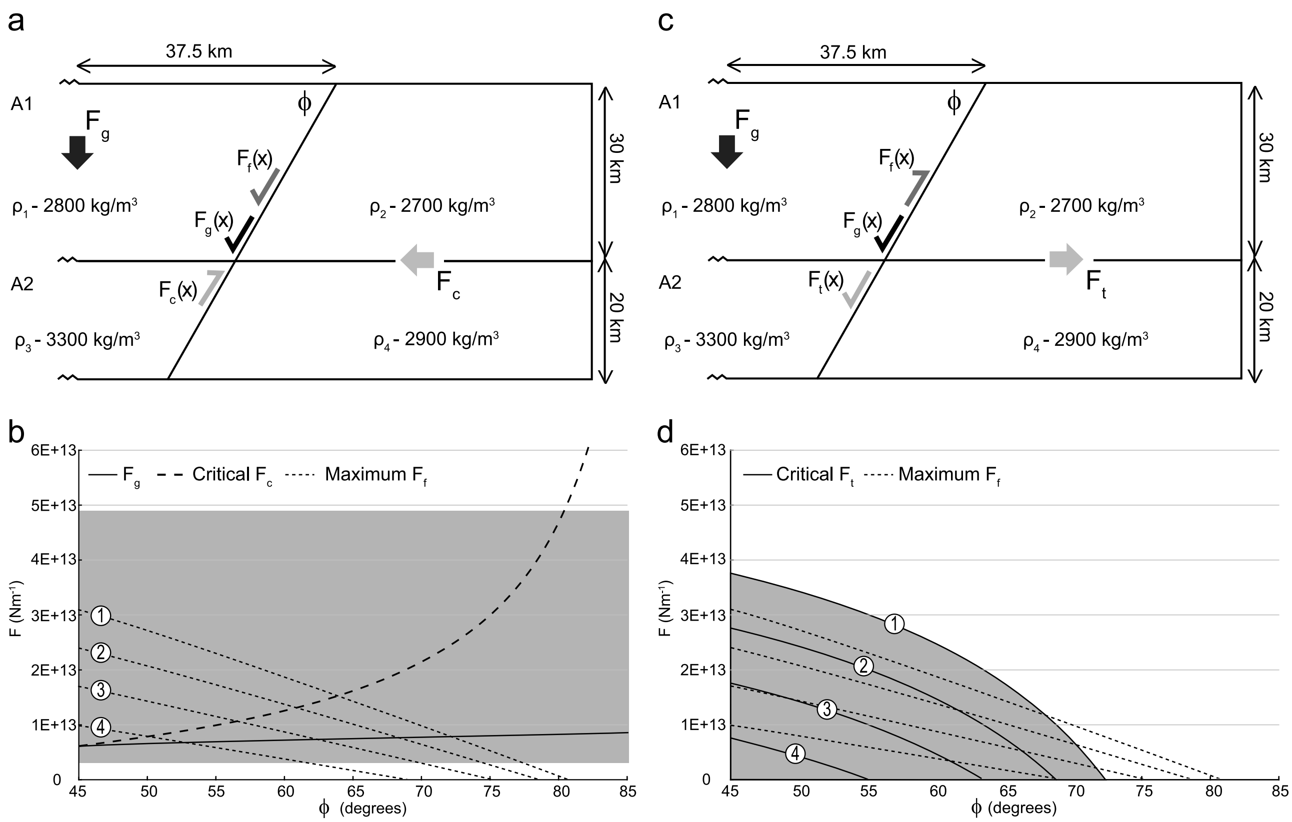

Figure 9. Schematic illustration of the simplified force-balance model of the Petermann Orogeny (Appendix A). (a) The system under compression, where F_g is the excess weight of the central wedge and is balanced by a horizontal compressive force, F_c. The components of F_g and F_c on a shear plane with dip angle ϕ are denoted as $F_g(x)$ and $F_c(x)$. The frictional force on the shear plane, $F_f(x)$, represents the shear strength of the system and is therefore opposite to the sense of motion. (b) Chart plotting F_g and the critical value of F_c required to uplift the wedge in the absence of friction ($F_f(x)$ is 0) against dip angle (ϕ). This shows the pronounced increase of the critical F_c value with dip angle. Also shown are four curves that display, for four particular values of F_c, the maximum possible frictional force ($F_f(x)$) under which uplift of the wedge can occur. Curve 1 is for $F_c = 5 \times 10^{13}\,\mathrm{Nm}^{-1}$, curve 2 is for $F_c = 4 \times 10^{13}\,\mathrm{Nm}^{-1}$, curve 3 is for $F_c = 3 \times 10^{13}\,\mathrm{Nm}^{-1}$, and curve 4 is for $F_c = 2 \times 10^{13}\,\mathrm{Nm}^{-1}$. The shaded area shows the range of reasonable tectonic forces, defined by typical slab-pull and ridge-push values from *Turcotte and Schubert* [2002]. (c) The system under tension is identical to the compressional case except that F_t is a horizontal tensional force, and therefore the sense of motion and the frictional force on the shear plane, $F_f(x)$, are reversed. In this case, $F_f(x)$ must balance both $F_g(x)$ and $F_t(x)$. (d) Using the four maximum frictional force $F_f(x)$ curves generated from the compressional model, four corresponding curves can be calculated to show the critical tensional force, F_t, required to reactivate the system. These curves define the potential stability field of the system (shaded) and show that if shear strength is reasonable, the system may be able to withstand significant tensional forces.

lower crust and the erosion of a heat producing layer in the upper crust, has led to a long-term increase in the integrated strength of the lithosphere by a factor of 2.85.

[57] However, given the uncertainty regarding the thermal structuring of the lithosphere prior to the Petermann Orogeny [*Camacho et al.*, 2002; *Neves et al.*, 2008; *Sandiford and McLaren*, 2002] it is useful also to calculate the influence of crust-mantle boundary uplift without the influence of crustal heating, and separate this from the influence of a reduction in crustal heat production. Using a 20 km thick heat producing layer at 2 $\mu\mathrm{Wm}^{-3}$ throughout the model, with the same changes in crustal thickness, yields a pre-Petermann Orogeny integrated lithospheric strength of 8.89×10^{13} Nm^{-1}, which with crustal thickening, reduces to 5.82×10^{13} Nm^{-1}, before uplift of the crust-mantle boundary increases this to a final strength of 1.27×10^{14} Nm^{-1}. This implies that uplift of the crust-mantle boundary has increased the integrated lithospheric strength of the lithosphere by a factor of 1.44, and that the remainder of the strengthening in the previous model, a further factor of 2, is due to the reduction in crustal heat production.

5.3. A Force-Balance Model of the Uplift of the Axial Zone and Its Subsequent Tectonic Stability

[58] The poorly constrained P-T-t data for the Petermann Orogeny [*Camacho et al.*, 1997; *Ellis and Maboko*, 1992; *Maboko et al.*, 1991; *Scrimgeour and Close*, 1999] allow

uplift of the axial zone at rates between 0.5 mm/yr, and 3.6 mm/yr. The rate of uplift has an important influence on the likelihood of postorogenic collapse along the major shear zones, because a slowly uplifted wedge of mantle will produce a conduction dominated thermal structure, as suggested for the Alice Springs Orogeny [*Sandiford*, 2002], and will cool faster than it is exhumed. In contrast, faster uplift will advect heat upward, as suggested for parts of the Musgrave Province [*Scrimgeour and Close*, 1999], causing localized heating and inhibiting the strengthening of the orogen. Of these, slow uplift is preferred, as it will progressively strengthen the lithosphere, and inhibit postorogenic collapse, better permitting the preservation of the uplifted mantle wedge for long periods [*Sandiford*, 2002]. However, faster uplift is feasible so long as the driving forces can maintain a dynamic equilibrium with the mass of the uplifted wedge until the lithosphere cools and strengthens.

[59] A simplified force-balance model of the crustal architecture details the forces required to maintain this dynamic equilibrium, and also assesses the vulnerability of the system to collapse under extension (Figure 9 and Appendix A). This model shows that, for dips between 50 and 70 degrees, the excess mass in the axial zone produces a gravitational force per unit length of between 4.45×10^{12} Nm^{-1} and 7.65×10^{12} Nm^{-1} (Figure 9b). Assuming frictionless shear planes, balancing this force by horizontal compressive forces alone requires a force of 5.31×10^{12} Nm^{-1} for a dip of 50 degrees, and 2.10×10^{13} Nm^{-1} for a dip of 70 degrees (Figure 9b). Both of these estimates are well within the range of plate tectonic forces [*Turcotte and Schubert*, 2002] and, given the influence of upward forces resulting from the erosion of the orogen hinterland and possibly delamination of the mantle lithosphere, uplift is geodynamically feasible.

[60] With frictionless shear planes, this model is inherently unstable, and will collapse as soon as horizontal compression relaxes. However, we can estimate the vulnerability of the system to collapse if a frictional force (i.e., a shear strength) is added to the force balance (Figure 9a). For a particular horizontal compressional force, the maximum shear strength under which uplift can occur is calculated, and a critical tensional force, below which the system is stable, can be derived (Appendix A and Figure 9d). Because it is derived from the maximum shear strength, this critical tensional force forms the upper limit to the stability field of the system for a given initial compressional force (Figure 9d). This simple test of the model demonstrates that with steeply dipping shear zones (>72°), the model is unstable, unless the initial compressive force was very large (>5×10^{13}), but that for dip angles shallower than ~65°, the system may be able to withstand significant extensional forces. Taking a moderate example, with a dip angle of 60°, and a wedge uplifted under a horizontal compressive force of 3×10^{13} Nm^{-1} (curve 3 in Figure 9b) a maximum shear strength of 8.7×10^{12} Nm^{-1} is predicted. This shear strength is comparable to the estimated strength of the lithosphere under thickening (Figure 8f) and is approximately 7% of the estimated strength of the lithosphere following the Petermann Orogeny (Figure 8h). The critical tensional force required to overcome this shear strength is 4.74×10^{12} Nm^{-1} (curve 3 in Figure 9d).

[61] We can compare this to the East African Rift, where estimates of the current stress field suggest tensional deviatoric stresses of 9–17 MPa [*Coblentz and Sandiford*, 1994; *Zoback*, 1992]. Assuming that this stress is uniformly distributed across a 100 km thick lithosphere yields a tensional force per unit length of between 0.9×10^{12} Nm^{-1} and 1.7×10^{12} Nm^{-1} which implies that the shear zones in our example would not be reactivated under the present tensional forces in the East African Rift.

5.4. True Strength of the System

[62] The Brace-Goetze lithospheric strength models and the simple force-balance model above demonstrate that this system may have sufficient strength to withstand both isostatic imbalances and a substantial tensional force. These calculations do not consider the full complexity of the geodynamic system, and in particular do not consider the influence of strain softening on the shear zones. As a result of shear heating and migmatization [*Camacho et al.*, 2001; *Scrimgeour and Close*, 1999] syndeformational weakening of these shear zones may have been intense. This transient weakening would be largely reversed on the cessation of deformation, but a significant amount of long-term strain softening may have been preserved by the system. The amount of this long-term strain softening is unknown, and it is therefore difficult to estimate the true strength of the system, and correspondingly, its ability to withstand tensional stress may be overestimated or, less likely, underestimated.

6. Conclusion

[63] Constrained potential field models of the crustal architecture of the Musgrave Province using new high-resolution data demonstrate that the regional gravity anomaly is in part accounted for by the thrusting of dense (2770 kgm^{-3}) granulite facies crust over less dense (2670 kgm^{-3}) amphibolite facies crust. However, uplift of the crust-mantle boundary beneath the axial zone of the province by 15–20 km is required to avoid an unrealistic density distribution in the near surface. This uplift is primarily accommodated on divergent transpressional shear zones that dip toward the hinterland at between 50 and 70 degrees, although these shear zones merge into more shallow dipping thrust faults at ~20 km depth.

[64] The location of the principal structures that accommodated uplift suggests the development or reactivation of lithospheric weaknesses close to the regions of maximum crustal curvature resulting from lithospheric thickening during the Petermann Orogeny. We interpret lithospheric failure due to the accumulation of stress in these regions, and possibly partial delamination of the mantle lithosphere, to have initiated the uplift of the axial zone of the province, by isolating this region from the downward forces associated with buckling of the lithosphere. Erosion and unroofing of the hinterland, and sedimentary loading of the foreland would accelerate the uplift of the axial zone of the province relative to the adjacent regions [e.g., *Avouac and Burov*, 1996; *Beaumont et al.*, 2000; *Burov and Toussaint*, 2007; *Hodges et al.*, 1998].

[65] The uplift of the entire crustal pile by 15 to 20 km can be expected to cause local lithospheric strengthening by two complementary phenomena: The replacement of rela-

tively weak lower crustal rocks with much stronger lithospheric mantle, and the erosion of an upper crust high in heat producing elements. Brace-Goetze lithospheric strength models indicate that the lithosphere may have been strengthened by a factor of 2.8 with both uplift and a reduction in crustal heat production, or by a factor of 1.44 with uplift alone. This local lithospheric strengthening, combined with the increasing mass of the uplifted wedge of mantle limits the development of the orogenic system, which, depending on the rate of uplift, will terminate either when lithospheric strengthening is sufficient to resist external stresses and support isostatic imbalances, or when a dynamic equilibrium is reached.

[66] The forces required to develop and sustain this dynamic equilibrium have been assessed using a simplified model of the orogen (Figure 9). This model shows that, for the moderately steep shear zones of our gravity models, the horizontal compressive force required to uplift the axial zone is tectonically reasonable, and that the system can be stable under reasonably strong tensional forces.

[67] This study demonstrates that the uplift of the crust-mantle boundary beneath an orogen is a feasible way to dramatically increase the integrated strength of the continental lithosphere, particularly where it is accompanied by a reduction in crustal heat production. This is an important process in both the Petermann Orogeny and the Alice Springs Orogeny, and may be a critical process for the tectonic stabilization of intraplate regions.

Appendix A

[68] The force required to produce uplift of the entire crustal pile by ~20 km is significant, and must be assessed for its tectonic likelihood. A simplified force-balance model of the crustal architecture of the Musgrave Province (Figure 9) was used to calculate the horizontal compressive force required to balance the gravitational load of the uplifted wedge. Uplift was assumed to have been accommodated on symmetrical, divergent shear zones with dip angles between 45° and 85°. As well as the simplified geometry, this model assumes that the fault planes are friction free, and that the blocks are rigid, i.e., there is no internal deformation or flexure.

[69] The magnitude of the gravitational load per unit length is directly proportional to the density contrast (s) and the area of the trapezium(s)

$$F_g = (\rho_1 - \rho_2) \times g \times A1 + (\rho_3 - \rho_4) \times g \times A2.$$

Balancing the component of the gravitational load on the shear plane, $F_g(x)$, against the component of the horizontal compressional force $F_c(x)$ on the same shear plane (Figure 9a) provides the relation

$$F_c = F_g \tan \varphi.$$

The dip of the shear plane, φ, is therefore most crucial variable in determining the magnitude of the critical compressional force required to support F_g, (Figure 9b).This model demonstrates that, in the absence of any other forces, this simplified version of the crustal architecture of the Musgrave Province requires horizontal compressive forces per unit length of the order of 1×10^{12} Nm^{-1} to 5×10^{13} Nm^{-1} to cause uplift of this 20 km thick wedge of lithospheric mantle into the lower crust. For dips less than ~75° these forces are well within the range of reasonable tectonic forces [*Turcotte and Schubert*, 2002], and the uplift of the wedge of lithospheric mantle is therefore geodynamically feasible, even for moderately steep shear planes.

[70] The vulnerability of this model to postorogenic collapse and subsequent tensional forces can also be assessed. By assuming that $F_c(x)$ is exactly balanced by the mass of the wedge, $F_g(x)$, and a frictional force, $F_f(x)$, the maximum possible shear strength of the system, above which uplift is not possible, can be calculated for a given F_c

$$F_f(x) = F_c(x) - F_g(x).$$

If the shear strength, $F_f(x)$, is greater than $F_g(x)$, the system can be considered stable under the cessation of horizontal compression, and the critical horizontal tensional force that will reactivate the system, F_t, can be calculated

$$F_t = \left(F_f(x) - F_g(x)\right) / \cos \varphi.$$

Using a range of F_c between 2×10^{13} Nm^{-1} and 5×10^{13} Nm^{-1}, the model is unstable for dip angles of greater than 55° in the former case, and 72° in the latter (Figure 9d). The potentially stable field, defined by the magnitude of the critical tensional force, F_t increases with shallower dip angles, and greater maximum shear strength. Although we cannot constrain the true shear strength of the Petermann Orogeny shear zones, the potential stability field predicted by this model is sufficiently large to suggest that the system may be able to withstand large tensional forces.

[71] **Acknowledgments.** This work was supported by Primary Industry and Resources South Australia (PIRSA) and Australian Research Council Linkage grant LP0560887. A. R. A. Aitken acknowledges the support of a Monash University postgraduate publication award. We thank Anya Reading, Chris Beaumont, Giampiero Iaffaldano, and an anonymous reviewer for their constructive reviews, which greatly improved the paper. We also thank Patrick Taylor and the associate editors for their editorial handling of the paper.

References

Aitken, A. R. A., and P. G. Betts (2008), High-resolution aeromagnetic data over central Australia assist Grenville-era (1300–1100 Ma) Rodinia reconstructions, *Geophys. Res. Lett.*, *35*, L01306, doi:10.1029/2007GL031563.

Aitken, A. R. A., and P. G. Betts (2009), Constraints on the Proterozoic supercontinent cycle from the structural evolution of the south-central Musgrave Province, central Australia, *Precambrian Res.*, *168*, 284–300, doi:10.1016/j.precamres.2008.10.006.

Aitken, A. R. A., P. G. Betts, B. F. Schaefer, and S. E. Rye (2008), Assessing uncertainty in the integration of aeromagnetic data and structural observations in the Deering Hills region of the Musgrave Province, *Aust. J. Earth Sci.*, *55*, 1127–1138, doi:10.1080/08120090802266600.

Avouac, J. P., and E. B. Burov (1996), Erosion as a driving mechanism of intracontinental mountain growth, *J. Geophys. Res.*, *101*, 17,747–17,769, doi:10.1029/96JB01344.

Beaumont, C., H. Kooi, and S. Willett (2000), Coupled tectonic-surface process models with applications to rifted margins and collisional orogens, in *Geomorphology and Global Tectonics*, edited by M. A. Summerfield, pp. 29–55, Wiley, Chichester, U. K.

Betts, P. G., D. Giles, G. S. Lister, and L. R. Frick (2002), Evolution of the Australian lithosphere, *Aust. J. Earth Sci.*, *49*, 661–695, doi:10.1046/j.1440-0952.2002.00948.x.

Biermeier, C., M. Wiesinger, K. Stuwe, D. A. Foster, H. J. Gibson, and A. Raza (2003), Aspects of the structural and late thermal evolution of the Redbank Thrust system, central Australia: Constraints from the Speares Metamorphics, *Aust. J. Earth Sci.*, *50*, 983–999, doi:10.1111/j.1400-0952.2003.01039.x.

Brace, W. F., and D. L. Kohlstedt (1980), Limits on lithospheric stress imposed by laboratory experiments, *J. Geophys. Res.*, *85*, 6248–6252, doi:10.1029/JB085iB11p06248.

Braun, J., and R. Shaw (2001), A thin-plate model of palaeozoic deformation of the Australian lithosphere: Implications for understanding the dynamics of intracratonic deformation, *Geol. Soc. Spec. Publ.*, *184*, 165–193.

Burov, E., and G. Toussaint (2007), Surface processes and tectonics: Forcing of continental subduction and deep processes, *Global Planet. Change*, *58*, 141–164, doi:10.1016/j.gloplacha.2007.02.009.

Camacho, A., and C. M. Fanning (1995), Some isotopic constraints on the evolution of the granulite and upper amphibolite facies terranes in the eastern Musgrave Block, central Australia, *Precambrian Res.*, *71*, 155–181, doi:10.1016/0301-9268(94)00060-5.

Camacho, A., and I. McDougall (2000), Intracratonic, strike-slip partitioned transpression and the formation of eclogite facies rocks: An example from the Musgrave Block, central Australia, *Tectonics*, *19*, 978–996, doi:10.1029/1999TC001151.

Camacho, A., W. Compston, M. McCulloch, and I. McDougall (1997), Timing and exhumation of eclogite facies shear zones, Musgrave Block, central Australia, *J. Metamorph. Geol.*, *15*, 735–751, doi:10.1111/j.1525-1314.1997.00053.x.

Camacho, A., I. McDougall, R. Armstrong, and J. Braun (2001), Evidence for shear heating, Musgrave Block, central Australia, *J. Struct. Geol.*, *23*, 1007–1013, doi:10.1016/S0191-8141(00)00172-3.

Camacho, A., B. J. Hensen, and R. Armstrong (2002), Isotopic test of a thermally driven intraplate orogenic model, Australia, *Geology*, *30*, 887–890, doi:10.1130/0091-7613(2002)030<0887:ITOATD>2.0.CO;2.

Cande, S. C., and J. C. Mutter (1982), A revised identification of the oldest sea-floor spreading anomalies between Australia and Antarctica, *Earth Planet. Sci. Lett.*, *58*, 151–160, doi:10.1016/0012-821X(82)90190-X.

Clarke, G. L., I. S. Buick, A. Y. Glikson, and A. J. Stewart (1995a), Structural and pressure-temperature evolution of host rocks of the Giles Complex, central Australia: Evidence for multiple high pressure events, *AGSO J. Aust. Geol. Geophys.*, *16*, 127–146.

Clarke, G. L., S. S. Sun, and R. W. White (1995b), Grenville-aged belts and associated older terranes in Australia and Antarctica, *AGSO J. Aust. Geol. Geophys.*, *16*, 25–39.

Clitheroe, G., O. Gudmundsson, and B. L. N. Kennett (2000), The crustal thickness of Australia, *J. Geophys. Res.*, *105*, 13,697–13,713, doi:10.1029/1999JB900317.

Coblentz, D. D., and M. Sandiford (1994), Tectonic stresses in the African plate: Constraints on the ambient lithospheric stress state, *Geology*, *22*, 831–834, doi:10.1130/0091-7613(1994)022<0831:TSITAP>2.3.CO;2.

Collins, W. J., and R. D. Shaw (1995), Geochronological constraints on orogenic events in the Arunta Inlier: A review, *Precambrian Res.*, *71*, 315–346, doi:10.1016/0301-9268(94)00067-2.

Cull, J. P. (1982), An appraisal of Australian heat-flow data, *BMR J. Aust. Geol. Geophys.*, *7*, 11–21.

Edgoose, C., A. Camacho, G. A. Wakelin-King, and B. A. Simons (1993), Kulgera, scale 1:250,000, sheet SG-53, Northern Territory Geol. Surv., Darwin, Northern Territory, Australia.

Edgoose, C. J., I. R. Scrimgeour, and D. F. Close (2004), Geology of the Musgrave Block, Northern Territory, *Rep.* 15, Northern Territory Geol. Surv., Darwin, Northern Territory, Australia.

Ellis, D. J., and M. A. H. Maboko (1992), Precambrian tectonics and the physiochemical evolution of the continental crust. Part I. The gabbro-eclogite transition revisited, *Precambrian Res.*, *55*, 491–506, doi:10.1016/0301-9268(92)90041-L.

Farquharson, C. G., M. R. Ash, and H. G. Miller (2008), Geologically constrained gravity inversion for the Voisey's Bay ovoid deposit, *Leading Edge*, *27*, 64–69, doi:10.1190/1.2831681.

Fishwick, S., and A. M. Reading (2008), Anomalous lithosphere beneath the Proterozoic of western and central Australia: A record of continental collision and intraplate deformation?, *Precambrian Res.*, *166*, 111–121, doi:10.1016/j.precamres.2007.04.026.

Flottmann, T., M. Hand, D. Close, C. Edgoose, and I. Scrimgeour (2005), Thrust tectonic styles of the intracratonic Alice Springs and Petermann orogenies, central Australia, *AAPG Mem.*, *82*, 538–557.

Forman, D. J. (1972), Petermann Ranges, Northern Territory, 1st ed., scale 1:250,000, sheet SG 52–7, Northern Territory Geol. Surv., Canberra.

Fullagar, P. K., G. A. Pears, and B. McMonnies (2008), Constrained inversion of geologic surfaces: Pushing the boundaries, *Leading Edge*, *27*, 98–105, doi:10.1190/1.2831686.

Glikson, A. Y., C. G. Ballhaus, G. L. Clarke, J. W. Sheraton, A. J. Stewart, and S. S. Sun (1995), Geological framework and crustal evolution of the Giles mafic/ultramafic complex and environs, western Musgrave Block, central Australia, *AGSO J. Aust. Geol. Geophys.*, *16*, 41–67.

Glikson, A. Y., A. J. Stewart, C. G. Ballhaus, G. L. Clarke, E. H. J. Feeken, J. H. Leven, J. W. Sheraton, and S. S. Sun (1996), Geology of the western Musgrave Block, central Australia, with particular reference to the mafic-ultramafic Giles Complex, *AGSO Bull.*, *239*, 41–68.

Goetze, C., and W. F. Brace (1972), Laboratory observations of high-temperature rheology of rocks, *Tectonophysics*, *13*, 583–600, doi:10.1016/0040-1951(72)90039-X.

Goetze, C., and B. Evans (1979), Stress and temperature in the bending lithosphere as constrained by experimental rock mechanics, *Geophys. J. R. Astron. Soc.*, *59*, 463–478.

Goleby, B. R., R. D. Shaw, C. Wright, B. L. N. Kennett, and K. Lambeck (1989), Geophysical evidence for "thick-skinned" crustal deformation in central Australia, *Nature*, *337*, 325–337, doi:10.1038/337325a0.

Goleby, B. R., B. L. N. Kennett, C. Wright, R. D. Shaw, and K. Lambeck (1990), Seismic reflection profiling in the Proterozoic Arunta Block, central Australia: Processing for testing models of tectonic evolution, *Tectonophysics*, *173*, 257–268, doi:10.1016/0040-1951(90)90222-T.

Gray, C. M. (1978), Geochronology of granulite facies gneisses in the western Musgrave Block, central Australia, *J. Geol. Soc. Aust.*, *25*, 403–414.

Gray, D., and A. R. A. Aitken (2007), Marla roadside gravity survey, *Rep. 2007/16*, Dep. of Primary Ind. and Resour., Adelaide, South Aust., Australia.

Gray, D., and M. Flintoft (2006), Musgrave Ranges roadside gravity survey, *Rep. 2006/15*, Dep. of Primary Ind. and Resour., Adelaide, South Aust., Australia.

Gray, D., A. R. A. Aitken, S. Petrie, and N. Gray (2007), Western Musgrave Ranges of South Australia roadside gravity survey, *Rep. 2007/19*, Dep. of Primary Ind. and Resour., Adelaide, South Aust., Australia.

Gray, D. R., and D. A. Foster (2004), Tectonic evolution of the Lachlan Orogen, southeast Australia: Historical review, data synthesis and modern perspectives, *Aust. J. Earth Sci.*, *51*, 773–817, doi:10.1111/j.1400-0952.2004.01092.x.

Haddad, D., A. B. Watts, and J. Lindsay (2001), Evolution of the intracratonic Officer Basin, central Australia: Implications from subsidence analysis and gravity modelling, *Basin Res.*, *13*, 217–238, doi:10.1046/j.1365-2117.2001.00147.x.

Hand, M., and M. Sandiford (1999), Intraplate deformation in central Australia, the link between subsidence and fault reactivation, *Tectonophysics*, *305*, 121–140, doi:10.1016/S0040-1951(99)00009-8.

Hodges, K., S. Bowring, K. Davidek, D. Hawkins, and M. Krol (1998), Evidence for rapid displacement on Himalayan normal faults and the importance of tectonic denudation in the evolution of mountain ranges, *Geology*, *26*, 483–486, doi:10.1130/0091-7613(1998)026<0483:EFRDOH>2.3.CO;2.

Hoskins, D., and N. Lemon (1995), Tectonic development of the eastern Officer Basin, central Australia, *Explor. Geophys.*, *26*, 395–402, doi:10.1071/EG995395.

Karner, G. D. (1991), Sediment blanketing and the flexural strength of extended continental lithosphere, *Basin Res.*, *3*, 177–185, doi:10.1111/j.1365-2117.1991.tb00127.x.

Kirby, J. F., and C. J. Swain (2006), Mapping the mechanical anisotropy of the lithosphere using a 2D wavelet coherence, and its application to Australia, *Phys. Earth Planet. Inter.*, *158*, 122–138, doi:10.1016/j.pepi.2006.03.022.

Kirby, S. H., and A. K. Kronenberg (1987), Rheology of the lithosphere, *Rev. Geophys.*, *25*, 1219–1244, doi:10.1029/RG025i006p01219.

Korsch, R. J., B. R. Goleby, J. H. Leven, and B. J. Drummond (1998), Crustal architecture of central Australia based on deep seismic reflection profiling, *Tectonophysics*, *288*, 57–69, doi:10.1016/S0040-1951(97)00283-7.

Kusznir, N. J., and G. D. Karner (1985), Dependence of the flexural rigidity of the continental lithosphere on rheology and temperature, *Nature*, *316*, 138–142, doi:10.1038/316138a0.

Kusznir, N. J., and R. G. Park (1984), The strength of intraplate lithosphere, *Phys. Earth Planet. Inter.*, *36*, 224–235, doi:10.1016/0031-9201(84)90048-7.

Lambeck, K. (1983), Structure and evolution of the intracratonic basins of central Australia, *Geophys. J. R. Astron. Soc.*, *74*, 843–886.

Lambeck, K., and G. Burgess (1992), Deep crustal structure of the Musgrave Block, central Australia: Results from teleseismic travel time anomalies, *Aust. J. Earth Sci.*, *39*, 1–19, doi:10.1080/08120099208727996.

Lambeck, K., G. Burgess, and R. D. Shaw (1988), Teleseismic travel time anomalies and deep crustal structure in central Australia, *Geophys. J.*, *94*, 105–124, doi:10.1111/j.1365-246X.1988.tb03431.x.

Lavier, L. L., and M. S. Steckler (1997), The effect of sedimentary cover on the flexural strength of continental lithosphere, *Nature*, *389*, 476–479, doi:10.1038/39004.

Lindsay, J. (2002), Supersequences, superbasins, supercontinents: Evidence from the Neoproterozoic-early Palaeozoic basins of central Australia, *Basin Res.*, *14*, 207–223, doi:10.1046/j.1365-2117.2002.00170.x.

Lindsay, J. F., and J. H. Leven (1996), Evolution of a Neoproterozoic to Palaeozoic intracratonic setting, Officer Basin, South Australia, *Basin Res.*, *8*, 403–424, doi:10.1046/j.1365-2117.1996.00223.x.

Maboko, M. A. H., I. S. Williams, and W. Compston (1991), Zircon U-Pb chronometry of the pressure and temperature history of granulites in the Musgrave Ranges, central Australia, *J. Geol.*, *99*, 675–697, doi:10.1086/629532.

Maboko, M. A. H., I. McDougall, P. K. Zeitler, and I. S. Williams (1992), Geochronological evidence for ~530–550 Ma juxtaposition of two Proterozoic metamorphic terranes in the Musgrave Ranges, central Australia, *Aust. J. Earth Sci.*, *39*, 457–471, doi:10.1080/08120099208728038.

Major, R. B., and C. H. H. Conor (1993), The Musgrave Block, in *The Geology of South Australia*, vol. 1, *The Precambrian*, *Geol. Surv. of South Aust. Bull. Ser.*, vol. 54, edited by J. F. Drexel, W. P. Priess, and A. J. Parker, pp. 156–167, Geol. Surv. of South Aust., Adelaide, South Aust., Australia.

McLaren, S., M. Sandiford, and R. Powell (2005), Contrasting styles of Proterozoic crustal evolution: A hot-plate tectonic model for Australian terranes, *Geology*, *33*, 673–676, doi:10.1130/G21544.1.

McLean, M., and P. G. Betts (2003), Geophysical constraints of shear zones and geometry of the Hiltaba Suite granites in the western Gawler Craton, Australia, *Aust. J. Earth Sci.*, *50*, 525–541, doi:10.1046/j.1440-0952.2003.01010.x.

McQueen, H. W. S., and K. Lambeck (1996), Determination of crustal structure in central Australia by inversion of traveltime residuals, *Geophys. J. Int.*, *126*, 645–662.

Neil, E. A., and G. A. Houseman (1999), Rayleigh-Taylor instability of the upper mantle and its role in intraplate orogeny, *Geophys. J. Int.*, *138*, 89–107, doi:10.1046/j.1365-246x.1999.00841.x.

Neves, S. P., A. Tommasi, A. Vauchez, and R. Hassani (2008), Intraplate continental deformation: Influence of a heat-producing layer in the lithospheric mantle, *Earth Planet. Sci. Lett.*, *274*, 392–400, doi:10.1016/j.epsl.2008.07.040.

Pysklywec, R. N., and C. Beaumont (2004), Intraplate tectonics: Feedback between radioactive thermal weakening and crustal deformation driven by mantle lithosphere instabilities, *Earth Planet. Sci. Lett.*, *221*, 275–292, doi:10.1016/S0012-821X(04)00098-6.

Ranalli, G., and D. C. Murphy (1987), Rheological stratification of the lithosphere, *Tectonophysics*, *132*, 281–295, doi:10.1016/0040-1951(87)90348-9.

Regenauer-Lieb, K., R. F. Weinberg, and G. Rosenbaum (2006), The effect of energy feedbacks on continental strength, *Nature*, *442*, 67–70, doi:10.1038/nature04868.

Regenauer-Lieb, K., G. Rosenbaum, and R. F. Weinberg (2008), Strain localisation and weakening of the lithosphere during extension, *Tectonophysics*, *458*, 96–104, doi:10.1016/j.tecto.2008.02.014.

Sandiford, M. (1999), Mechanics of basin inversion, *Tectonophysics*, *305*, 109–120, doi:10.1016/S0040-1951(99)00023-2.

Sandiford, M. (2002), Low thermal Peclet number intraplate orogeny in central Australia, *Earth Planet. Sci. Lett.*, *201*, 309–320, doi:10.1016/S0012-821X(02)00723-9.

Sandiford, M., and M. Hand (1998), Controls on the locus of intraplate deformation in central Australia, *Earth Planet. Sci. Lett.*, *162*, 97–110, doi:10.1016/S0012-821X(98)00159-9.

Sandiford, M., and S. McLaren (2002), Tectonic feedback and the ordering of heat producing elements within the continental lithosphere, *Earth Planet. Sci. Lett.*, *204*, 133–150, doi:10.1016/S0012-821X(02)00958-5.

Sandiford, M., M. Hand, and S. McLaren (2001), Tectonic feedback, intraplate orogeny and the geochemical structure of the crust: A central Australian perspective, *Geol. Soc. Spec. Publ.*, *184*, 195–218.

Scrimgeour, I. R., and D. F. Close (1999), Regional high-pressure metamorphism during intracratonic deformation: The Petermann Orogeny, central Australia, *J. Metamorph. Geol.*, *17*, 557–572, doi:10.1046/j.1525-1314.1999.00217.x.

Scrimgeour, I. R., D. F. Close, and C. J. Edgoose (1999), Petermann Ranges, Northern Territory, 2nd ed., scale 1:250,000, sheet SG 52–7, Northern Territory Geol. Surv., Darwin, Northern Territory, Australia.

Shaw, R. D., P. Wellman, P. Gunn, A. J. Whitaker, C. Tarlkowski, and M. Morse (1995), "Australian crustal elements" map: A geophysical model for the tectonic framework of the continent, *AGSO Res. Newsl.*, *23*, 1–3.

Stephenson, R., and K. Lambeck (1985), Isostatic response of the lithosphere with in-plane stress: Application to central Australia, *J. Geophys. Res.*, *90*, 8581–8588, doi:10.1029/JB090iB10p08581.

Sun, S. S., and J. W. Sheraton (1992), Zircon U/Pb chronology, tectonothermal and crust-forming events in the Tomkinson Ranges, Musgrave Block, central Australia, *AGSO Res. Newsl.*, *17*, 9–11.

Sun, S. S., J. W. Sheraton, A. Y. Glikson, and A. J. Stewart (1996), A major magmatic event during 1050–1080 Ma in central Australia, and an emplacement age for the Giles Complex, *AGSO Res. Newsl.*, *24*, 13–15.

Talwani, M. (1965), Computation with the help of a digital computer of magnetic anomalies caused by bodies of arbitrary shape, *Geophysics*, *30*, 797–817, doi:10.1190/1.1439654.

Talwani, M., and J. R. Heirtzler (1964), *Computation of Magnetic Anomalies Caused by Two-Dimensional Structures of Arbitrary Shape*, Stanford Univ. Press, Palo Alto, Calif.

Talwani, M., J. L. Worzel, and M. Landisman (1959), Rapid gravity computations for two-dimensional bodies with application to the Mendochino submarine fracture zone, *J. Geophys. Res.*, *64*, 49–59.

Tingate, P. R., and I. R. Duddy (2002), The thermal history of the eastern Officer Basin (South Australia): Evidence from apatite fission track analysis and organic maturity data, *Tectonophysics*, *349*, 251–275, doi:10.1016/S0040-1951(02)00056-2.

Turcotte, D. L., and G. Schubert (2002), *Geodynamics*, 2nd ed., 456 pp., Cambridge Univ. Press, Cambridge, U. K.

Veevers, J. J. (1990), Tectonic-climatic supercycle in the billion-year plate-tectonic eon: Permian Pangean icehouse alternates with Cretaceous dispersed-continents greenhouse, *Sediment. Geol.*, *68*, 1–16, doi:10.1016/0037-0738(90)90116-B.

Wade, B. P., M. Hand, and K. M. Barovich (2005), Nd isotopic and geochemical constraints on provenance of sedimentary rocks in the eastern Officer Basin, Australia: Implications for the duration of the intracratonic Petermann Orogeny, *J. Geol. Soc.*, *162*, 513–530, doi:10.1144/0016-764904-001.

Wade, B. P., K. M. Barovich, M. Hand, I. R. Scrimgeour, and D. F. Close (2006), Evidence for early Mesoproterozoic Arc magmatism in the Musgrave Block, central Australia: Implications for Proterozoic Crustal Growth and Tectonic Reconstructions of Australia, *J. Geol.*, *114*, 43–63, doi:10.1086/498099.

Wade, B. P., D. E. Kelsey, M. Hand, and K. M. Barovich (2008), The Musgrave Province: Stitching north, west and south Australia, *Precambrian Res.*, *166*, 370–386, doi:10.1016/j.precamres.2007.05.007.

Walter, M. R., J. J. Veevers, C. R. Calver, and K. Grey (1995), Late Proterozoic stratigraphy in the Centralian Superbasin, Australia, *Precambrian Res.*, *73*, 173–195, doi:10.1016/0301-9268(94)00077-5.

Wellman, P. (1988), Development of the Australian Proterozoic crust as inferred from gravity and magnetic anomalies, *Precambrian Res.*, *40–41*, 89–100, doi:10.1016/0301-9268(88)90062-9.

White, R. W., G. L. Clarke, and D. R. Nelson (1999), SHRIMP U-Pb zircon dating of Grenville-age events in the western part of the Musgrave Block, central Australia, *J. Metamorph. Geol.*, *17*, 465–481, doi:10.1046/j.1525-1314.1999.00211.x.

Won, I. J., and M. Bevis (1987), Computing the gravitational and magnetic anomalies due to a polygon: Algorithms and Fortran subroutines, *Geophysics*, *52*, 232–238, doi:10.1190/1.1442298.

Young, D. N., N. Duncan, A. Camacho, P. A. Ferenczi, and T. L. A. Madigan (2002), Ayers Rock, scale 1:250,000, sheet SG 52–8, 2nd ed., Northern Territory Geol. Surv., Darwin, Northern Territory, Australia.

Zhao, J., M. T. McCulloch, and R. T. Korsch (1994), Characterisation of a plume-related approximately 800 Ma magmatic event and its implications for basin formation in central-southern Australia, *Earth Planet. Sci. Lett.*, *121*, 349–367, doi:10.1016/0012-821X(94)90077-9.

Ziegler, P. A., J. D. Van Wees, and S. Cloetingh (1998), Mechanical controls on collision-related compressional intraplate deformation, *Tectonophysics*, *300*, 103–129, doi:10.1016/S0040-1951(98)00236-4.

Zoback, M. L. (1992), First-and second-order patterns of stress in the lithosphere: The World Stress Map Project, *J. Geophys. Res.*, *97*, 11,703–11,728, doi:10.1029/92JB00132.

A. R. A. Aitken, P. G. Betts, and R. F. Weinberg, School of Geosciences, Monash University, PO Box 28E, Melbourne, Vic 3800 Australia. (alan.aitken@sci.monash.edu.au)

D. Gray, Minerals, Petroleum and Energy Group, Primary Industries and Resources South Australia, Level 7, 101 Grenfell St., Adelaide, SA 5001, Australia.